Analysis and Comparison of System Performance Using Different Modulation Schemes for Long-haul Optical Systems and Fiber-to-The-Home Passive Optical Networks

Analysis and Comparison of System Performance Using Different
Modulation Schemes for Long-haul Optical Systems and Fiber-to-
The-Home Passive Optical Networks

By

Xianming Zhu, B.Sc.

A Thesis

Submitted to the School of Graduate Studies

in Partial Fulfillment of the Requirements

for the Degree of Master of Applied Science

McMaster University

MASTER OF APPLIED SCIENCE (2006)   McMaster University

Electrical and Computer Engineering   Hamilton, Ontario

TITLE: Analysis and Comparison of System Performance Using Different Modulation Schemes for Long-haul Optical Systems and Fiber-to-The-Home Passive Optical Networks

AUTHOR: Xianming Zhu, B. Sc. (Peking University)

SUPERVISORS: Professor Shiva Kumar, Professor Xun Li (Co-supervisor)

Number of Pages: xiii, 108

Abstract

Analytical expressions for the propagation impairments due to various noise sources in long-haul optical systems and fiber-to-the-home passive optical networks have been obtained. Extensive comparison has been made in this thesis for systems based on different modulation formats, and the advantage of one over the other is clearly stated.

For long-haul fiber optical communication systems with inline amplifiers, we have studied the statistical properties of various noise sources in systems based on differential phase-shift keying (DPSK) such as the linear phase noise induced by the amplifier spontaneous emission (ASE) noise, the intra-channel four-wave mixing (IFWM) and the nonlinear phase noise induced by the interplay between ASE noise and fiber Kerr nonlinearity. The error probability of the system based on DPSK is evaluated semi-analytically. In addition, the error probability of the system based on on-off keying (OOK) is calculated taking into account the effects of ASE noise, and the intra-channel nonlinearities such as IFWM and intra-channel cross-phase modulation (IXPM). Comparison of the performance of systems based on DPSK and OOK is made thereafter.

For fiber-to-the-home passive optical networks without inline active photonic devices, different modulation formats have been examined for the downstream and upstream data to enable full-duplex transmission. The statistical properties of Rayleigh backscattering in single-source bi-directional optical systems have been studied including the effects of the high speed external modulation signal and the laser phase noise for systems based on DPSK and OOK. The error probabilities for systems using OOK/OOK topology and DPSK/OOK topology for downstream/upstream transmission have been evaluated and compared.

In addition, the interplay of the amplifier spontaneous emission noise, fiber nonlinearity and dispersion has been examined starting from the nonlinear Schrödinger equation on the receiver current fluctuation. The variance of the current noise has been evaluated analytically using the two dimensional perturbation theory.

Acknowledgement

I would like to express my sincere thanks to my supervisor Dr. Shiva Kumar, for his enthusiastic guidance, understanding and encouragement throughout the process of this research work.

I would also like to thank my co-supervisor Dr. Xun Li, and our group leader Dr. Wei-Ping Huang, for their generous help not only about my research work but also about my life and careers.

Thanks to all the fellows in the photonics research group in McMaster University for the helpful discussions and the happy times I spent here.

My deepest gratitude belongs to my parents and my brother, for their constant love and support.

Contents

List of Figures

1

Introduction

1.1 Long-Haul Optical Systems with Different Modulation Formats

Until recently, with the advent of erbium-doped fiber amplifiers (EDFAs), optical communication systems are based on on-off keying (OOK) in either non-return-to-zero (NRZ) or return-to-zero (RZ) format. For high-bit-rate transmission systems based on OOK, the nonlinear pulse-to-pulse interaction is one of the main limiting factors. The fiber nonlinearity shifts the frequencies of the interacting pulses, which, in turn, results in timing jitter and intersymbol interference [1]. The nonlinear interaction between adjacent pulses in the dispersive systems is described in terms of intra-channel cross-phase modulation (IXPM). The adjacent pulse causes phase modulation of the probe pulse due to IXPM, which shifts the leading pulse to the red spectral region and the trailing pulse to the blue spectral region [1]. This translates into timing fluctuations due to fiber dispersion. The IXPM-induced pulse-to-pulse interaction can be reduced with strong dispersion management, however, one still can see some amplitude jitter in the 1's and ghost

1

pulses in the 0's. When two or more adjacent pulses of the same channel interact, because of the pulse spreading due to dispersion, the nonlinear mixing of the pulses gives rise to ghost pulses on both sides of the pulses. This process is called intra-channel four wave mixing (IFWM).

In recent years because of the higher demanding on the performance of long-haul transmission, optical systems based on differential phase-shift keying (DPSK) resumed great attention because of the 3-dB sensitivity advantage over on-off keying (OOK) in the linear regime [2]. In addition, for the dispersive nonlinear system, the impact of IXPM is greatly reduced for systems based on DPSK, since the timing shift caused by a left neighboring pulse is cancelled by a corresponding right pulse. This is because the timing jitter due to IXPM is not phase sensitive. However, the power fluctuations caused by IFWM are phase sensitive and thus do not cancel, leading to performance degradations in systems based on DPSK. In addition, the power fluctuations caused by amplified spontaneous emission (ASE) noise are translated into phase fluctuations by the fiber nonlinearity, resulting in phase jitter, which is now known as Gordon-Mollenauer effect [3]. For systems with zero dispersion, the nonlinear phase noise could be very large, and Gordon and Mollenauer concluded that this effect would ultimately limit the usefulness of phase-modulation schemes. However, for highly dispersive systems with phase-modulation, several results show that the chromatic dispersion can reduce the ASE induced nonlinear phase noise due to self-phase modulation (SPM) [4-5]. However, for strongly pulse overlapped transmission

2

systems, the ASE induced nonlinear phase noise due to IXPM might become important because of the strong overlap between adjacent pulses due to pulse spreading.

The motivation of Chapter 3 of this thesis is to examine the effects of dispersion on the nonlinear phase noise including both SPM and IXPM effects in a long-haul fiber-optic transmission systems. We have derived a semianalytical formula, for the first time to our knowledge, for the error probability (BER) taking into account IFWM, linear phase noise and nonlinear phase noise. In addition, a semi-analytical formula for the error probability has been given for systems based on OOK, considering the effects of ASE noise and intrachannel nonlinear effects such as IXPM and IFWM. Our results[1,2] show that, to reach a BER of 10^{-9}, the difference of the required signal-to-noise ratio (SNR) between DPSK and OOK depends critically on the launch power. For the launch power under -3 dBm, the difference of the SNR between DPSK and OOK is around 3 dB, which is consistent with the result from the linear theory [2]; however, for the launch power of 0 dBm, this difference of SNR increases to 6 dB, and the difference grows nonlinearly as the launch power increases.

_____

[1] Xianming Zhu and Shiva Kumar, "Error Probabilities in Optical Transmission Systems Based on DPSK and OOK," Coherent Optical Technologies and Applications, OSA Topical Meeting, Whistler, BC, Canada, June 2006.

[2] Xianming Zhu, Shiva Kumar and Xun Li, "Analysis and Comparison of Impairments in DPSK and OOK systems based on the Error Probability," *Applied Optics*, vol. 45, No. 26, September, 2006.

1.2 Rayleigh Backscattering in BiDirectional FTTH Passive Optical networks

For the Fiber-to-the-Home passive optical networks, bidirectional optical systems with different sources operating at separate wavelengths are currently used in the Optical Line Terminal (OLT) and Optical Network Unit (ONU) for the downstream and upstream data transmission. Recently single-source bidirectional optical systems have been proposed and studied to reduce the cost for a single customer by replacing the source in ONU for upstream transmission with a reflecting modulator, preventing the stabilization of the local laser in ONU [8]. In addition, different modulation formats have been proposed and demonstrated for the single-source structure. In Ref. [9] it is shown that the bidirectional transmission using OOK for both downstream and upstream is feasible. In Ref. [10] a topology known as frequency-shift keying (FSK)/OOK in which FSK for downstream and OOK for upstream is presented.

In Chapter 4 of this thesis, we examined the statistical properties of Rayleigh backscattering caused by OOK signal and DPSK signal, taking into account the laser phase noise and the high-speed nonstationary modulation signals. The effects of Rayleigh backscattering on the system performance have been studied and the error probability for bidirectional systems using OOK/OOK

topology and DPSK/OOK topology are evaluated. Our results[3,4] show that , to

acquire the given BER of 10^{-9}, the required receiver power in bidirectional optical

systems using DPSK/OOK topology is around 9 dBm lower than that in the

system using OOK/OOK topology if non-return-to-zero (NRZ) signal is used. In

addition, the effect of duty cycle on the system performance has also been studied,

and our results show that, for both OOK/OOK and DPSK/OOK topology, using

return-to-zero (RZ) signal can lead to significant performance improvement

compared with the non return-to-zero (NRZ) signal, and the improvement for

OOK/OOK topology is larger than that of DPSK/OOK topology.

1.3 Fluctuations Caused by the Interplay of ASE Noise,

Dispersion and Fiber Nonlinearity

Erbium-doped fiber amplifiers (EDFAs) show their great potential in the

advanced optical communication systems because of their large, polarization-

independent gain and high efficiency [11]. For systems using inline optical

amplifiers, it has been shown that the interaction between fiber Kerr nonlinearity

and amplifier spontaneous emission (ASE) noise causes enhancement of the

---

[3] Xianming Zhu and Shiva Kumar, "Effects of Rayleigh Backscattering in Single Source Bidirectional Optical Systems Using DPSK and OOK Formats," submitted to *IEEE/OSA Journal of Lightwave Technology*.

[4] Xianming Zhu and Shiva Kumar, "Rayleigh Backscattering in Fiber-to-The-Home Passive Optical Networks," Ontario Photonics Consortium (OPC), London, ON, May 2006.

relative intensity noise (RIN) within the signal baseband in the anomalous dispersion regime or zero group velocity dispersion through the modulation-instability (MI) process [12-13]. However, in the normal dispersion regime, the variance of RIN can be reduced since the ASE spectrum does not experience the MI gain. In fact, in this case, the measured variance of RIN is smaller than that of a linear fiber-optic system [14-15].

In Chapter 5 of this thesis, we examined the current fluctuations of the detected pulse caused by the interplay between fiber nonlinearity and ASE noise in a dispersive system using a two-dimensional perturbation theory. We treat fiber nonlinear coefficient and the power spectral density of the amplifier noise as small parameters and use statistical techniques to calculate the variance of current fluctuations. Our results[5] show that for anomalously dispersive nonlinear systems, the current fluctuation is larger than that for a linear system with the same dispersion map, which is consistent with that in [12]; while for the normally dispersive nonlinear systems, the current fluctuation becomes smaller as compared with that of the linear system, consistent with Ref. [15].

1.4 Thesis Structure

---

[5] Xianming Zhu and Shiva Kumar, "Two Dimensional Perturbation Theory for the Current Fluctuations Caused by Nonlinearity and Amplified Spontaneous Emission Noise in On-Off Keying Optical Transmission Systems," to be submitted to *IEEE/OSA Journal of Lightwave Technology*.

In Chapter 2, the literature background on long-haul and bidirectional fiber-to-the-home (FTTH) passive optical networks (PONs) is given.

In Chapter 3, the statistical properties of nonlinear phase noise for long-haul systems based on DPSK is studied with the second-order perturbation technique, and the semi-analytical models for the error probability in both systems based on DPSK and OOK are derived and the system performance are compared.

In Chapter 4 the statistical properties of Rayleigh Backscattering is studied for FTTH PONs caused by DPSK and OOK signals. The error probability (BER) of the bidirectional system using OOK/OOK topology and DPSK/OOK topology are evaluated and compared.

In Chapter 5, a two-dimensional theory is developed to study the power fluctuations caused by the interaction of amplifier spontaneous emission noise (ASE) and the fiber nonlinearities.

Chapter 6 gives the conclusion and future direction of this thesis.

2

Research Background

2.1   Long-haul Fiber-optic Communication Systems Optical

Systems

Until recently, fiber-optic systems based on intensity modulation (IM) or on-off

keying (OOK) with direct detection (DD) have been extensively deployed. As

wavelength-division-multiplexed (WDM) systems were pushed to higher levels of

performance, a number of advanced optical modulation formats have attracted

increased attention [16-18]. In contrast to OOK, phase-shift-keying (PSK) format

carries information in the optical phase. To detect the phase at receiver, a coherent

optical source serving as the local oscillator whose frequency and phase aligned to

the signal is required [19]. Although it is possible to align the phase in RF and

microwave frequency regimes, it is extremely hard to achieve it at optical

frequencies. However, if the phase of the previous bit is used as a reference for

the current bit, the requirement for the absolute phase reference by a coherent

source is avoided, and hence, such a scheme is called differential-phase-shift keying (DPSK). Recently, DPSK format has attracted significant attention for long-haul optical transmission systems [17-22].

Two commonly used RZ-DPSK transmitter setups are shown in Fig. 2-1 as of in Ref. [2]. The transmitters consist of a continuously oscillating laser followed by an external modulator. The phase modulation is performed either by a straight-line phase modulator (PM, Fig. 2-1a), or by a Mach-Zehnder modulator (MZM, Fig. 2-1b). A PM only modulates the phase of the optical field, resulting in a constant-envelope optical signal. Since the phase modulation does not occur instantaneously, a PM inevitably introduces chirp across bit transitions. The MZM consists of two waveguides with Y-branches. By applying a voltage between the two electrodes, the optical phase in the two waveguides rotates in different direction. If the modulation efficiencies of two waveguides are equal, the phase of the combined optical signal changes abruptly from 0 to π [20]. In addition, as shown in Fig. 2-1, a sinusoidally driven second modulator ("pulse carver") may be used to carve pulses out of the phase-modulated signal, thus generating RZ-DPSK.

The most commonly used receiver circuit to demodulate the DPSK signal is to use the DPSK balanced receiver. Fig. 2-2 shows the structure of the commonly used DPSK balanced receiver. The optical signal is first passed through a Mach-Zehnder delay-interferometer (DI), whose differential delay is equal to the bit period. The two output ports of the DI are connected to two

photodiodes using a balanced receiver. If b(t) is the optical signal before the balanced receiver, then the current $s(t)$ after the receiver assuming unit responsivity for the photodiodes is given by:

$$s(t) = |b(t) - b(t-T)|^2 - |b(t) + b(t-T)|^2$$
$$= 4|b(t)||b(t-T)|\cos\Delta\Phi,$$

(2-1)

where $\Delta\Phi$ is the phase difference between the two adjacent bits.
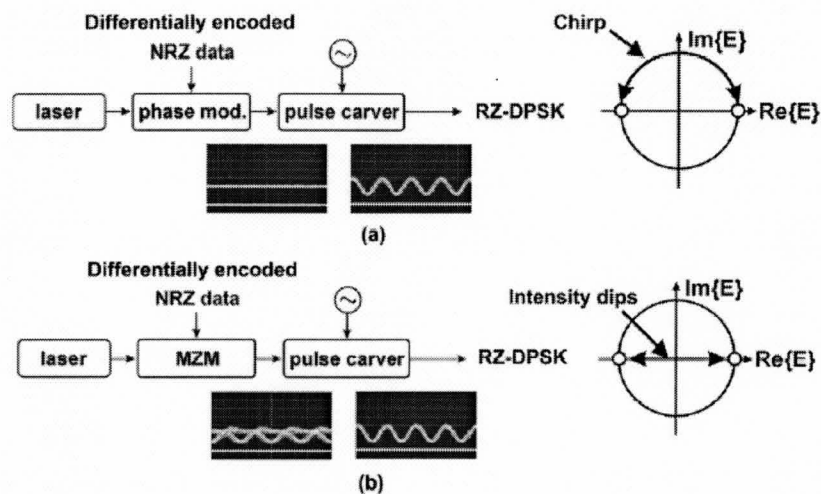
Fig. 2-1 Two typical DPSK transmitters. (a) Implementation with phase modulation. (b) Implementation with Mach-Zehnder modulator.
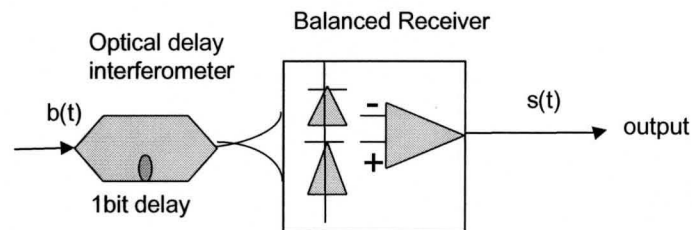
Fig. 2-2 DPSK Balanced Receiver

Using the balanced receiver, systems based on DPSK require the optical

signal-to-noise ratio (OSNR) 3 dB less than those based on OOK if the system is

linear [2]. This is because the symbol distance in DPSK is increased by $\sqrt{2}$

compared with OOK for the same average optical power. This improvement is

important because it allows the fiber launch power to be lower to avoid the

deleterious effects of fiber nonlinearities. In addition, as the timing jitter caused

by IXPM is not phase sensitive, the timing shift caused by a left neighboring

pulse is cancelled by a corresponding right pulse, greatly reducing the impact of

IXPM on systems based on DPSK. However, the ghost pulses induced by IFWM

do not cancel. In Refs. [6] and [7], the ghost pulses induced by IFWM on the

given bit slot were studied numerically by exhausting all the possible bit patterns,

and results show that DPSK signal also has higher tolerance to IFWM than OOK

signal [6].

However, for systems with periodic optical amplifiers to compensate the

fiber loss, as the fiber's refractive index is dependent upon the optical power

through fiber Kerr nonlinearity, the power fluctuations caused by ASE noise are

translated into phase fluctuations, resulting in phase jitter, which is known as

Gordon-Mollenauer effect [3]. The limitations due to nonlinear phase noise on

systems using phase modulation (PSK and DPSK) was first studied by Gordon

and Mollenauer. A simple Gaussian model of the nonlinear phase noise was

examined in Ref. [3] ignoring the fiber dispersion. By computing the linear and

nonlinear phase variance, they arrived at the result that the errors are minimized when the total nonlinear phase shift is in the neighborhood of 1 rad. After that, extensive studies of the statistical properties of nonlinear phase noise have been carried on. For zero-dispersion fiber-optic communication systems, the probability density function (p.d.f) has been evaluated analytically in the literatures [21-22]. In Refs. [21] and [22] the nonlinear phase noise is modeled as the summation of a noncentral χ^2 random variable with two degrees of freedom in a zero dispersion system, and for a large number of fiber spans and inline amplifiers, the nonlinear phase becomes an integration of the square of the Wiener process. The characteristic function for such process was evaluated in [23], and the p.d.f of the nonlinear phase noise is the inverse Fourier transform of its characteristic function [24]. The results in Ref. [21] showed a non-Gaussian distribution of the nonlinear phase noise alone, however, in [22] the deviations of the phase noise from the Gaussian curves of the same variance becomes almost unnoticeable for large signal-to-noise ratio (SNR).

For systems based on DPSK with balanced receiver, a decision as to whether the received symbol is '1' or '0' is made on the basis of whether the receiver output at the sampling instant is positive or negative. The receiver output at the sampling instant described in Eq. (2-1) can be written as:

$$s = R\cos(\Delta\phi), \tag{2-2}$$

where R and $\Delta\phi$ are random variables with arbitrary probability density function (p.d.f). Under the assumption that the p.d.f of the phase $\Delta\phi$ is an even symmetric function, and each transmitted symbol is statistically independent of its predecessors, the probability of error Pe is identical for a "1" or "0" transmission. An error is made if the received signal is negative, when the transmitted signal is positive. Thus the error probability can be described as:

$$Pe = \int_{-\infty}^{0} q_s(r)dr, \qquad (2\text{-}3)$$

where $q_s(r)$ is the p.d.f of the balanced receiver output s.

Following the procedure similar to Jain [25], the characteristic function $\Psi_s(v)$ of the random variable S is introduced, and its cumulative distribution function is [26]:

$$C(x) = \int_{-\infty}^{x} q_s(r)dr = \frac{1}{2} - \frac{1}{\pi} \int_{0}^{\infty} \text{Im}[\Psi_s(v)e^{-jvx}]\frac{dv}{v}, \qquad (2\text{-}4)$$

where $\Psi_s(v) = E[\exp(jvs)] = E[\exp(jvR \cos \Delta\phi)]$, $\text{Im}\{\cdot\}$ denotes the imaginary part of the complex variable, and $E\{\cdot\}$ denotes the expectation. From Eqs. (2-3) and (2-4), it follows that [25]:

$$
\begin{aligned}
Pe = C(0) &= \frac{1}{2} - \frac{1}{\pi} \int_{0}^{\infty} \text{Im}[\Psi_s(v)]\frac{dv}{v} = \frac{1}{2} - \frac{1}{\pi} \int_{0}^{\infty} E[\sin(vR \cos \Delta\phi)]\frac{dv}{v} \\
&= \frac{1}{2} - \frac{2}{\pi} \sum_{n=0}^{\infty} (-1)^n E \int_{0}^{\infty} \frac{J_{2n+1}(vR)}{v}dv \cdot \cos[(2n+1)\Delta\phi] \\
&= \frac{1}{2} - \frac{2}{\pi} \sum_{n=0}^{\infty} \frac{(-1)^n}{(2n+1)} E\{\cos[(2n+1)\Delta\phi]\}.
\end{aligned}
\qquad (2\text{-}5)
$$

13

It can be seen from Eq.(2-5) that the probability depends only on the phase of the received signal [25].

2.1.1   Nonlinear Phase Noise

For zero-dispersion systems based on DPSK, the phase of the received signal is mainly deteriorated by the linear phase noise from the ASE noise and the nonlinear phase noise from the interaction of ASE and fiber Kerr nonlinearity. Ho [27] has studied the error probability of the zero-dispersion systems with different models for the linear phase noise and the nonlinear phase noise: 1) Gaussian approximation of the nonlinear phase noise, and the independence of the linear phase noise and nonlinear phase noise; 2) independent approximation of the linear and nonlinear phase noise with the exact p.d.f of the nonlinear phase noise, and 3) the exact model which takes into account the dependence of the linear and nonlinear phase noise as non-Gaussian variables. The result in [27] showed that for zero-dispersion systems, the Gaussian approximation gives a smaller p.d.f than the exact model, and thus underestimates the error probability of DPSK signals with nonlinear phase noise. However, as the mean nonlinear phase shift increases, the difference between the approximation model and the exact model decreases.

For real long-haul fiber-optic transmission systems with dispersive fibers, to find the exact p.d.f of the nonlinear phase noise taking the combined effects of ASE, Kerr nonlinearity and chromatic dispersion is really complicated, and so far

14

there exists no analytical results in the literature when all the above effects are combined. In Refs. [4] and [5], the variance of the ASE induced nonlinear phase noise has been evaluated analytically for highly dispersive systems with single pulse. And their results show that, for large highly dispersive systems, the nonlinear effects are suppressed, and the phase noise is reduced to the linear value. However, with large number of pulses transmitting in the system, because of the pulse spreading in the dispersive system, the ASE induced nonlinear phase noise due to IXPM could become important in this case. In Chapter 3 of this thesis, we calculated the variance of the ASE induced nonlinear phase noise including the effects of SPM and IXPM in the fiber-optic transmission systems with arbitrary system configuration. Then we modeled the nonlinear phase noise as a Gaussian process and calculated the error probability of systems based on DPSK.

2.1.2   Linear Phase Noise

The linear phase noise represents the phase noise induced by the narrowband signal and the normal noise processes caused by ASE. The statistical properties of the envelope and phase of the narrowband normal noise, as well as the additive narrowband signal with the normal noise process have been studied exclusively in [26].

For the narrowband normal noise, it can be written as:

$$N(t) = N_c(t)\cos\omega_0 t + N_s(t)\sin\omega_0 t = A(t)\cos[\omega_0 t - \theta(t)], \qquad (2\text{-}6)$$

where ω_0 is the central frequency of the noise, $A(t)$ and $\theta(t)$ are the envelope and

phase of the normal process, and they are related with N_c and N_s by:

$$A(t) = \sqrt{N_c^2 + N_s^2}, \text{ and } \theta(t) = \tan^{-1}(N_s/N_c) \tag{2-7}$$

With the assumption that $N(t)$ is a zero-mean stationary normal process,

the joint first-order distribution density for N_c and N_s is given in [26]:

$$W_1(N_c, N_s) = \frac{e^{-(N_c^2 + N_s^2)/2\Psi}}{2\pi\Psi}, \tag{2-8}$$

where Ψ is the power of the noise per dimension,

$$\Psi = \overline{N_c^2} = \overline{N_s^2} \tag{2-9}$$

Inserting Eq. (2-7) into (2-8), the joint distribution density of the envelope and the

phase is achieved:

$$w_1(A, \theta) = W_1[N_c(A, \theta), N_s(A, \theta)]\left|\frac{\partial(N_c, N_s)}{\partial(A, \theta)}\right| = \frac{Ae^{-A^2/2\Psi}}{2\pi\Psi}, \tag{2-10}$$

where $0 \le A < \infty, \quad 0 \le \theta \le 2\pi$.

Assume ω_c is the central frequency of the signal, and the signal is written as:

$$S(t) = A(t)\cos(\omega_c t - \psi) \tag{2-11}$$

The additive narrowband signal and the normal noise process can be written as

[26]:

$$\begin{aligned} V(t) &= S(t) + N(t) = A\cos(\omega_c t - \psi) + N_c \cos\omega_0 t + N_s \sin\omega_c t \\ &= V_c(t)\cos\omega_0 t + V_s(t)\sin\omega_0 t = A'\cos(\omega_0 t - \theta'), \end{aligned} \tag{2-12}$$

16

where

$$\begin{bmatrix} N_c \\ N_s \end{bmatrix} = \begin{bmatrix} V_c - A\cos\varphi \\ V_s + A\sin\varphi \end{bmatrix} = \begin{bmatrix} A'\cos\theta' - A\cos\varphi \\ A'\sin\theta' + A\sin\varphi \end{bmatrix} \tag{2-13}$$

and $\varphi = (\omega_c - \omega_0)t - \psi$.

Inserting Eq.(2-13) into (2-8), the joint distribution density of the envelope and phase is reached:

$$w_1(A',\theta') = \frac{A'}{2\pi\Psi}\exp\left\{-\left[A'^2 + A^2 - 2A'A\cos(\theta'-\varphi)\right]/2\Psi\right\} \tag{2-14}$$

Integrating Eq. (2-14) over the envelope, the distribution density of the phase of the additive narrowband signal and normal noise process is [26]:

$$w_1(\theta') = \frac{1}{2\pi} + \frac{1}{\pi}\sum_{m=1}^{\infty}\frac{\Gamma(m/2+1)}{m!}\rho^m\,_1F_1\left[m/2, m+1, -\rho^2\right]\cos(m\theta'), \tag{2-15}$$

where $\rho^2 = A^2/2\Psi$ is the signal-to-noise ratio, $_1F_1[\ ]$ is the confluent hypergeometric function.

2.2   Single Source Bidirectional FTTH Passive optical networks

The most widely deployed broadband solutions today are digital subscriber line (DSL) and cable modem (CM) networks, both of which are built on top of existing copper communication infrastructure not optimized for data traffic [33]. However, data traffic is increasing at an unprecedented rate nowadays; neither DSL nor CM networks can keep up with such high demand. As optical fiber is capable of delivering bandwidth-intensive integrated voice, data and video

17

services at distances beyond 20 km in the subscriber access network, fiber-to-the-home (FTTH) technology based on passive optical networks (PON) becomes one of the main research objectives in the "broad-band for all" concept that encourages the development of optical access infrastructure. A PON is a point-to-multi-point optical network with no active elements in the transmission path, and all transmissions in a PON are performed between an optical line terminal (OLT) which resides in the central office, and the optical network units (ONU) located at the end-user location [33]. The key element in PON is the ONU as it has a direct impact on the cost per customer. Many methods have been proposed to simplify the structure of ONU, thus reduce the cost per capital. For example, only one single fiber is used for both upstream and downstream transmission in order to reduce network size and connection complexity of the outside plant [34]; the laser source at the ONU is eliminated to avoid its stabilization and provisioning, while a single reflective semiconductor optical amplifier (RSOA) is used at the ONU to function as a modulator and detector [9]. The feasibility of single source bi-directional system is demonstrated in Ref. [9] using RSOA at the bit rate of 1.25 Gb/s experimentally. Fig. 2-3 shows the basic structure of the bi-directional optical systems using double sources and single source, respectively. An interface circuit is implemented at OLT and ONU to separate the received downstream signal and update date.
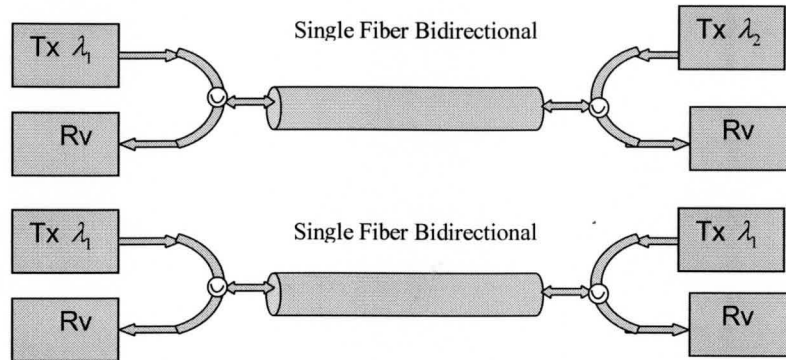
Fig. 2-3 Single Fiber Strategies

2.2.1 Rayleigh Backscattering

Rayleigh scattering (RB) results from the small scale fluctuations in the refractive index of the fiber due to density and composition variations frozen into the fiber during manufacturing. As the Rayleigh scattering field is in all directions, a fraction of the backscattered field is scattered within the numerical aperture of the fiber, it is captured and travels in the backward direction. The backscattered Rayleigh Backscattering field interferes with the upstream signal, causing serious deteriorations to the detected signal and thus limiting the receiver sensitivity. Fig. 2-4 shows the interface between the Rayleigh Backscattering field and the upstream signal.
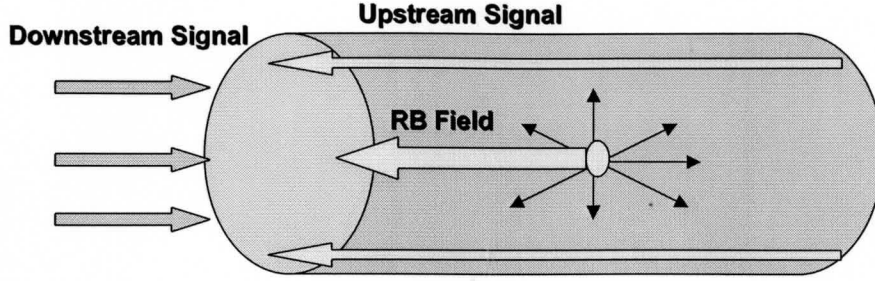
Fig. 2-4 Rayleigh Backscattering Field

For the single-mode optical fibers, the forward pulse energy is attenuated at a rate of α, where α is the fiber loss coefficient, and it depends on position z:

$$E(z) = E(0)\exp(-\alpha z) \tag{2-16}$$

The energy scattered at a distance element dz situated at z is:

$$dE_S(z, z+dz) = E(z)\alpha_s(z)dz, \tag{2-17}$$

where α_s is the Rayleigh scattering loss coefficient.

Define the capture fraction $S(z)$ as the proportion of the total energy scattered at z which is recaptured by the fiber in the return direction, the backscattering energy recaptured at the launch end $dE_{BS}(z, z+dz)$ is [35]:

$$dE_{BS}(z, z+dz) = E(0)\alpha_s(z)S(z)\exp(-2\alpha z)dz \tag{2-18}$$

The backscatter factor $S(z)$ denoting the ratio of the backscattered power to the energy launched into the fiber is accurately modeled in Ref. [37] of the dependence on the parameters of the fiber which involves only the near-field distribution of HE_{11} mode.

20

To evaluate the statistical properties of Rayleigh backscattering field, the single-mode fiber of length L is partitioned into N scatter sections, where $\Delta l = L / N$ is in the order of an optical wavelength λ and therefore is large compared with the correlation distance of refractive index fluctuations in the fiber. If the coherence length of incident light is larger than the section length Δl, the backscattered field vector from a scattering section shows circular complex Gaussian (ccG) statistics, and the field vectors from distinct scatter sections are statistically independent [37]. The backscattered signal $\Delta \varepsilon_b(t, z)$ received at the fiber input from a scatter section located at z is given in Ref. [37] under the assumption of polarization preservation as

$$\Delta \varepsilon_b(t, z) = \varepsilon_s(t - 2z / \upsilon)e^{-\alpha z}e^{-2j\beta z}\Delta \rho(z) \qquad (2\text{-}19)$$

where ε_s is the source field, α is the loss coefficient, β is the propagation constant, ν is the group velocity, $\Delta \rho(z)$ is the backscattering coefficient denoting the fraction of the scattered field from a section located at z in the backward direction, which is a zero-mean ccG random variable. And the total backscattered field is the superposition of all the contributions from different sections:

$$\varepsilon_b(t) = \sum_{n=1}^{N}\Delta \varepsilon_b(t, n\Delta l) \qquad (2\text{-}20)$$

Define the differential backscattering coefficient $\rho(z) = \lim_{\Delta l \to 0} \Delta \rho(z) / \Delta l$, Eq. (2-20) can be written as:

$$\varepsilon_b(t) = \int_0^L \varepsilon_s(t - \frac{2z}{\upsilon})e^{-\alpha z}e^{-j2\beta z}\rho(z)dz, \qquad (2\text{-}21)$$

where $\rho(z)$ is modeled as a zero-mean ccG random process [37]:

$$\langle \rho^*(z_1)\rho(z_2) \rangle = \alpha_s S \cdot \delta(z_1 - z_2) \qquad (2\text{-}22)$$

Based on Eqs.(2-21) and (2-22), the power spectral densities of the Rayleigh backscattering field and the total received field which includes the interaction of the reflected field and the Rayleigh backscattering field have been studied in Refs. [36] and [37]. For the source field which is affected by the laser phase noise and the non-stationary modulation signal, the source field as well as the Rayleigh backscattering field becomes non-stationary random process. it is shown in [37] that the auto-correlation function of Rayleigh backscattering field becomes wide-sense stationary even if the modulation signal is non-stationary, under the assumption that the source coherence time and the symbol duration is small compared with the fiber round-trip delay:

$$\tau_c \ll T_L, \qquad T_s \ll T_L \qquad (2\text{-}23)$$

2.2.2   Modulation Formats in FTTH Passive Optical Networks

Using single-source bidirectional structure in FTTH PONs, the laser source is eliminated at ONU, avoiding its stabilization and provisioning, and, if possible, all ONUs become wavelength independent to fit in a transparent wavelength-division-multiplexing (WDM) scenario of a future FTTH network. Some ONU

models, that avoid the local generation of light, have been lately demonstrated by using different modulation formats for upstream and downstream transmission.

In ref. [9] a bidirectional structure using OOK format for both downstream and upstream transmission was implemented and proved feasible. A reflective semiconductor optical amplifier (RSOA) is used in the ONU acting as modulator and photo-detector. The bias current determines whether the RSOA is working as a modulator or detector. As the intensity modulated signal (on-off keying signal) does not contain the carrier information needed for the upstream transmission, the OOK/OOK structure was considered operating in burst mode. Downstream data and upstream carrier are sent from the OLT time multiplexed in a single burst. The first burst section is downstream data and then, after a guard band, unmodulated optical carrier is sent for upstream modulation purpose. Upstream data is modulated by the RSOA, amplified, and sent back to the OLT; there, the optical circulator routes the incoming signal to the detection branch and isolates the laser source [9].

In Ref. [10] a topology known as frequency-shift keying (FSK)/OOK in which FSK for downstream and OOK for upstream is presented. Since the intensity of the downstream FSK signal is constant, the direct intensity modulation of the signal at ONU is possible, which simplifies the transmission protocol. However, because of the incoherent FSK receiver is used in Ref. [10], the signal bandwidth is larger than that required by OOK or DPSK. In addition, DPSK format has the well-known advantage of 3 dB signal-to-noise ratio (SNR)

over FSK and OOK to reach the given BER [2]. Therefore, in Chapter 4 of this thesis, we analyze the error probability of a bidirectional system based on DPSK/OOK topology and compare it with that of a system based on OOK/OOK topology.

2.3   Modulation instability in Optical Fibers

Modulation instability (MI) is a process in which weak perturbations from the steady state grow exponentially as a result of the interplay between the nonlinearity and the group-velocity dispersion, breaking up the cw or quasi-cw radiation into a train of ultrashort pulses. It has been shown in [28] that the stability of the perturbed steady state solution of the nonlinear Schrödinger equation depends critically on the fiber dispersion. The wave number of the perturbed field to the steady state solution becomes imaginary in the case of anomalous group-velocity dispersion ($\beta_2 < 0$), and the perturbed field grows exponentially with the propagation distance z [28]. The modulation instability in a glass fiber was explicitly analyzed by Hasegawa and Brinkman [29], and was experimentally verified by Tai et al [30].

A well-known effect of the modulation instability caused by the interplay between fiber nonlinearity and the anomalous group velocity dispersion is to cause the enhancement of the noise spectrum, which leads to the increase of the relative intensity noise (RIN) within the signal bandwidth compared to the linear system [31]. However, for the nonlinear optical systems with normal dispersion

fiber, the amplitude of the RIN is reduced when compared to the linear system, and this effect has been verified both experimentally by Hui and O'Sullivan [32] by measuring the RIN spectrum, and analytically by Midrio [15] for the cw wave. This is because the noise photons do not experience MI gain in the normal dispersion regime. In chapter 5 of this thesis, we have developed a two dimensional perturbation theory to describe the interaction between noise spectrum and fiber nonlinearity, and obtained analytical expressions for the variance of the current fluctuations in a quasi-linear system.

3

Long-Haul Fiber-Optic Communication Systems with Different Modulation Formats

The major impairments to the optical transmission systems using differential phase-shift keying (DPSK) format are caused by three noise sources: intra-channel four-wave mixing (IFWM), linear phase noise and nonlinear phase noise. The impact of intra-channel four-wave mixing (IFWM) has been studied extensively on the system performance for return-to-zero (RZ)-DPSK modulation format [6-7]. In addition, the power fluctuations caused by the amplified spontaneous emission (ASE) noise are translated into phase fluctuations by the fiber nonlinearity, resulting in phase jitter, which is known as Gordon-Mollenauer effect [3]. In highly dispersive systems, the ASE induced nonlinear phase noise due to self-phase modulation (SPM) becomes much smaller than that in systems with no dispersion [4-5]. However, ASE induced nonlinear phase noise due to

intra-channel cross-phase modulation (IXPM) could become important in this case. Previously, the combined effects of Kerr nonlinearity and the ASE noise have been studied by Mecozzi for systems based on OOK and DPSK formats with zero-dispersion [13, 38]. In this chapter, we examine the effects of dispersion on the nonlinear phase noise including both SPM and IXPM effects in a long-haul fiber-optic transmission system. We have derived a semi-analytical formula, for the first time to our knowledge, for the error probability taking into account IFWM, linear phase noise and nonlinear phase noise. Our results show that the variance of the nonlinear phase noise becomes much smaller than that of IFWM in the presence of pre-compensation.

For the transmission systems based on on-off keying (OOK), the major noise sources are ASE noise and intra-channel nonlinear effects such as intra-channel four-wave mixing (IFWM) and intra-channel cross-phase modulation (IXPM). By considering these two kinds of noise sources, a semi-analytical formula of the error probability (BER) has been given, and the performance of OOK based on this formula has been studied. The results show that, in order to reach a BER of 10^{-9}, the difference of the required signal-to-noise ratio (SNR) between DPSK and OOK depends critically on the launch power. For the launch power under -3 dBm, the difference of the SNR between DPSK and OOK is around 3 dB, which is consistent with the result from the linear theory [2]; however, for the launch power of 0 dBm, this difference of SNR increases to 6 dB,

and the difference grows nonlinearly as the launch power increases. This is because the impact of nonlinearity in DPSK format is much smaller than that in OOK format for the given launch power.

The schematic of the system we consider in the chapter is shown in Fig. 3-1. The transmission fiber is composed of a 40 km of standard single-mode fiber with positive dispersion D_1, nonlinear coefficient $\gamma_1 = 2.5$ $W^{-1}km^{-1}$ and loss $\alpha_1 = 0.2$ dB/km, followed by a negative dispersion fiber of the same length with dispersion D_2, nonlinear coefficient $\gamma_2 = 10.0$ $W^{-1}km^{-1}$ and loss $\alpha_2 = 0.2$ dB/km. After each transmission fiber, an amplifier is inserted with $n_{sp} = 1$ to compensate the fiber loss. Pre- and post- compensation fibers are inserted at the transmitter and receiver end to compensate the residual dispersion, with dispersion coefficient $D_{pre} = D_{post} = -100$ ps/nm.km, nonlinear coefficient $\gamma_2 = 10$ $W^{-1}km^{-1}$, and loss $\alpha_{pre} = \alpha_{post} = 0.5$ dB/km. The total length of the compensation fibers is chosen such that the accumulative dispersion at the receiver is zero, and the portion of pre-compensation fiber is chosen to optimize the system performance.

Fig. 3-1 Schematic of a dispersion managed optical transmission system.

In this chapter, Section 3.1 gives the mathematical analysis of the nonlinear phase noise in highly dispersive systems and the error probability of DPSK format including three noise sources in dispersion- managed systems. In Section 3.2 we give the semi-analytical expression for the error probability of OOK format including ASE and intra-channel nonlinear effects. Section 3.3 gives the simulation results using the theory developed in section 3.1 and 3.2. The analytical model of the nonlinear phase noise including the effects of SPM and IXPM is validated by Monte-Carlo simulation of the nonlinear Schrödinger equation, then the comparison between the performance of OOK and DPSK formats is made. Section 3.4 gives the concluding remarks of the chapter.

3.1   Error Probability for DPSK Modulation Format

Using DPSK balanced receiver, the error probability depends only on the received phase noise as shown in Eq. (2-5). As the received signal is impaired by three noise sources for systems based on DPSK: 1) intra-channel four-wave mixing (IFWM) occurring between pulses in the given bit pattern; 2) linear phase noise due to ASE, and 3) ASE induced nonlinear phase noise due to SPM and IXPM, thus the phase of the received signal can be written as:

$$
\begin{aligned}
\Delta\phi &= \phi(t) - \phi(t - T_b), \\
&= [\phi_L(t) + \phi_{NL}(t) + \phi_{IFWM}(t)] - [\phi_L(t - T_b) + \phi_{NL}(t - T_b) + \phi_{IFWM}(t - T_b)], \quad (3\text{-}1) \\
&= \Delta\phi_{L+NL} + \Delta\phi_{IFWM}
\end{aligned}
$$

where $\phi_L(t)$ represents the linear phase fluctuation due to ASE, $\phi_{NL}(t)$ represents

the ASE induced nonlinear phase fluctuation due to SPM and IXPM, $\phi_{IFWM}(t)$ is

the phase noise induced by the IFWM impairment, and

$$\Delta\phi_{L+NL} = \phi_L(t) + \phi_{NL}(t) - \phi_L(t - T_b) - \phi_{NL}(t - T_b),$$ (3-2)

$$\Delta\phi_{IFWM} = \phi_{IFWM}(t) - \phi_{IFWM}(t - T_b).$$ (3-3)

And the error probability for systems based on DPSK is evaluated by Eq. (2-5):

$$Pe = \frac{1}{2} - \frac{2}{\pi}\sum_{n=0}^{\infty}\frac{(-1)^n}{(2n+1)}E\{\cos[(2n+1)\Delta\phi]\}$$
$$= \frac{1}{2} - \frac{2}{\pi}\sum_{n=0}^{\infty}\frac{(-1)^n}{(2n+1)}E\{\cos[(2n+1)\cdot(\Delta\phi_{L+NL} + \Delta\phi_{IFWM})]\}$$ (3-4)

In the analytical model, we assume the three phase noise sources are independent. Although the linear phase noise and nonlinear phase noise is slightly dependent on each other, however, as shown in [27], the difference of the independent approximation and exact model is small, and this difference decreases as the average nonlinear phase increases. In Ref. [27] expressions for the error probability was obtained by adding the linear phase and nonlinear phase together; and in [7] the error probability was obtained by adding the linear phase noise and IFWM. In our research, we combine all the three noise sources and derive an expression for the error probability. For systems based on DPSK, the p.d.f of the linear and nonlinear phase is an even function, from Eq.(3-4), we have:

$$Pe = \frac{1}{2} - \frac{2}{\pi}\sum_{n=0}^{\infty}\frac{(-1)^n}{(2n+1)}E\{\cos[(2n+1)\Delta\phi_{L+NL}]\}\cdot E\{\cos[(2n+1)\Delta\phi_{IFWM}]\}.$$ (3-5)

30

3.1.1 Linear Phase Noise

The linear phase noise represents the random phase of a sinusoidal signal plus Gaussian noise. The statistical properties of the envelope and phase of the additive narrowband signal and normal noise process have been studied in [26]. The p.d.f of the linear phase noise ϕ_L is derived in [26]:

$$p(\phi_L) = \frac{1}{2\pi} + \frac{1}{\pi} \sum_{m=1}^{\infty} C_m \cos(m\phi_L), \tag{3-6}$$

where $C_m = \frac{\sqrt{\pi \rho_s}}{2} e^{-\rho_s/2} \left[I_{(m-1)/2}\left(\frac{\rho_s}{2}\right) + I_{(m+1)/2}\left(\frac{\rho_s}{2}\right) \right]$, and ρ_s is SNR which is equal to the signal power at the decision point divided by the noise power .

Since each transmitted bit is statistically independent of its precedent, $\phi_L(t)$ and $\phi_L(t - T_b)$ are independent, and have the same p.d.f. In the same way, the nonlinear phase $\phi_{NL}(t)$ and $\phi_{NL}(t - T_b)$ are independent, and have the same p.d.f.

3.1.2 Nonlinear Phase Noise

The ASE induced nonlinear phase noise was shown to be one of the major impairments to systems based on DPSK to limit the performance, and it was first studied in [3]. The statistical property of the nonlinear phase noise has been studied extensively for systems with zero dispersion [21-22]; however, there exists no analytical results for the p.d.f of the nonlinear phase for a dispersive system. In [5] it is shown that the ASE induced nonlinear phase noise due to SPM

is small in a highly-dispersive system while the linear phase noise is dominant, however, the ASE induced nonlinear phase noise due to IXPM could become important. In this chapter, we derived the analytical model for the variance of the nonlinear phase noise due to SPM and IXPM using the first-order perturbation technique [39], and then model the nonlinear phase noise as a Gaussian process to get its p.d.f from the first and second order of its moment. Within the regime that the first-order perturbation theory is valid for the system, the nonlinear phase noise has the same statistical properties as the energy fluctuation, which is a Gaussian process, thus modeling the nonlinear phase noise as a Gaussian process is valid for our research..

For systems with structure as shown in Fig. 3-1 where the pre- and post-compensation fibers are used to compensate the dispersion of the transmission fiber, we consider the nonlinear phase fluctuation caused by an amplifier located at position z_i. We assume the initial condition at the transmitter is:

$$u_k(0,t) = \sqrt{P_0} \exp\left(-\frac{(t-kT_b)^2}{2T_0^2}\right) = \sqrt{\frac{E_0}{T_{\mathit{eff}}}} \exp\left(-\frac{(t-kT_b)^2}{2T_0^2}\right) \tag{3-7}$$

where T_b is the bit interval, T_0 is the half-width at 1/e-intensity point, P_0 is the launch power, T_{eff} is the effective pulse width defined as the ratio of energy and peak power which is equal to $\sqrt{\pi}T_0$, and E_0 is the pulse energy defined as:

$E_0 = P_0 T_{\mathit{eff}}$.

The solution for the linear Schrödinger equation at location z_i (0th order solution) is:

$$u_k^{(0)}(z_i,t) = \sqrt{\frac{E_0}{\sqrt{\pi}T_{z_i}}} \exp\left[-\frac{(t-kT_b)^2(1+jC_{z_i})}{2T_{z_i}^2} + j\theta_{z_i}\right],$$ (3-8)

where $E_0 = P_0\sqrt{\pi}T_0$ is the launched energy at the transmitter, T_0 is the half width at 1/e-intensity, T_b is the bit interval, and

$$T_{z_i} = \frac{\sqrt{T_0^4 + S_{z_i}^2}}{T_0}, \quad C_{z_i} = \frac{S_{z_i}}{T_0^2}, \quad E_{z_i} = E_0,$$ (3-9)

$$\theta_{z_i} = \frac{1}{2}\tan^{-1}\left(\frac{S_{z_i}}{T_0^2}\right), \quad S_{z_i} = \int_0^{z_i}\beta_2(s)ds,$$ (3-10)

Consider the field in location z_i as the new initial condition; we obtain the 0th order solution for nonlinear Schrödinger Equation for the chirped Gaussian pulses [28]:

$$u_k^{(0)}(z,t) = \sqrt{\frac{E_0}{\sqrt{\pi}T(z)}}e^{j(\theta_{z_i}+\theta(z))}\exp\left[-\frac{(t-kT_b)^2(1+jC(z))}{2T(z)^2}\right],$$ (3-11)

where

$$T(z) = \frac{\sqrt{\left(T_{z_i}^2 + C_{z_i}S(z)\right)+S^2(z)}}{T_{z_i}}$$ (3-12)

$$C(z) = \frac{S(z) + C_{z_i}T_{z_i}^2 + C_{z_i}^2S(z)}{T_{z_i}^2}$$ (3-13)

$$\theta(z) = \frac{1}{2}\tan^{-1}\left(\frac{S(z)}{T_{z_i}^2 + C_{z_i}S(z)}\right)$$ (3-14)

33

We expand the field u_k into a series:

$$u_k = u_k^{(0)} + \gamma u_k^{(1)} + \gamma^2 u_k^{(2)} + \cdots \qquad (3\text{-}15)$$

u_k is the electric-field envelope at bit slot k, and $u_k^{(m)}$ denotes the m th-order

solution, and γ is a small parameter usually taken to be the fiber nonlinear

coefficient.

By taking the nonlinearity as perturbations to the linear Schrödinger

equation, we obtain the equation including SPM and IXPM to the first order [39]:

$$j\frac{\partial u_k^{(1)}}{\partial z} - \frac{\beta_2(z)}{2}\frac{\partial^2 u_k^{(1)}}{\partial t^2} = -\exp\left(-\int_0^z \alpha(s)ds\right) \times \qquad (3\text{-}16)$$

$$\left[\left|u_k^{(0)}\right|^2 + 2\sum_{l=-N/2}^{N/2}\left|u_l^{(0)}\right|^2\right]u_k^{(0)}, l \neq k, \quad l,k = -N/2,\cdots,N/2,$$

where N+1 is the total number of bits, $\beta_2(z)$ is the dispersion profile, and $\alpha(s)$ is

the loss/gain profile. The first term in the square bracket denotes SPM

contributions, whereas the second term denotes the IXPM contributions from all

other pulses to the pulse slot k.

First we solve Eq. (3-16) considering only the second term on the right

hand side, which represents the effects of IXPM. The solution corresponding to

SPM is quite similar.

For IXPM only, the separation between the two pulses is $l \cdot T_b$

($l = -N/2,\cdots,N/2.$), then the right hand side of Eq. (3-16) can be written as:

$$
\begin{aligned}
F(z,t) &= \sum_{l=-N/2}^{N/2} \left\{ -2\exp(-w(z)) \left| u_l^{(0)} \right|^2 u_0^{(0)} \right\} \\
&= -2\sum_{l=-N/2}^{N/2} \left\{ \exp(-w(z)) \frac{E_0}{\sqrt{\pi T(z)}} \exp\left[-\frac{(t-l\cdot T_b)^2}{2T(z)^2} \right] \cdot \sqrt{\frac{E_0}{\sqrt{\pi T(z)}}} e^{j(\theta_{z_i}+\theta(z))} \exp\left[-t^2 \frac{(1+jC(z))}{2T(z)^2} \right] \right\} \\
&= \eta(z) \sum_{l=-N/2}^{N/2} \exp\left[-\sum_{m=1}^{2} (t-D_{m,l}(z))^2 R_m(z) \right],
\end{aligned}
$$

$$(3\text{-}17)$$

where

$$
w(z) = \int_0^z \alpha(s)\,ds, \qquad \eta(z) = -2\exp(-w(z)) \frac{E_0}{\sqrt{\pi T(z)}} \sqrt{\frac{E_0}{\sqrt{\pi T(z)}}} e^{j(\theta_{z_i}+\theta(z))}
$$

$$(3\text{-}18)$$

$$
\begin{cases}
R_1(z) = \dfrac{1}{T(z)^2}, & R_2(z) = \dfrac{(1+jC(z))}{2T(z)^2} \\
D_{1,l} = l\cdot T_b, & D_{2,l} = 0
\end{cases}
$$

$$(3\text{-}19)$$

Following the method in [39], we can get the solution for the 1st order perturbation term caused by IXPM:

$$
u_0^{(1),IXPM}(z,t) = -j \int_{z_i}^{z} \frac{\eta(y)\exp\left\{ -\bar{R}\cdot\tau^2 - \dfrac{(t-\bar{D})^2}{\delta} \right\}}{\sqrt{\delta(z,y)R(y)}}\,dy,
$$

$$(3\text{-}20)$$

where
$$
\begin{cases}
\bar{R} = \dfrac{R_1 R_2}{R_1 + R_2}, & R = R_1 + R_2 \\
\bar{D} = \dfrac{\tau R_2}{R_1 + R_2}, & \delta(z,y) = \dfrac{1-2jR[S(z)-S(y)]}{R}
\end{cases}
$$

$$(3\text{-}21)$$

In the same way, we can get the 1st order perturbation term caused by SPM:

$$
u_0^{(1),SPM}(z,t) = -j \int_{z_i}^{z} \frac{\eta'(y)}{\sqrt{\delta(z,y)R(y)}} \cdot \exp\left\{ -\frac{t^2}{\delta} \right\} dy
$$

$$(3\text{-}22)$$

where $\eta'(z) = -\exp(-w(z)) \dfrac{E_0}{\sqrt{\pi T(z)}} \sqrt{\dfrac{E_0}{\sqrt{\pi T(z)}}} e^{j(\theta_{z_i}+\theta(z))}$

$$(3\text{-}23)$$

Thus the total solution at the end of the transmission line can be written as:

$$u_0(L,t) = u_0^{(0)}(L,t) + \gamma u_0^{(1),SPM}(L,t) + \gamma u_0^{(1),IXPM}(L,t) \tag{3-24}$$

Inserting Eqs. (3-20) and (3-22) into (3-24), and after some algebra, we obtain the solution for the field in the 0th bit slot at the pulse center:

$$u_0(L) = \sqrt{\frac{E_{z_i}}{\sqrt{\pi}T(L)}} e^{j\left(\theta_{z_i} + \theta(L)\right)} \left\{1 + j\gamma E_{z_i} h(z_i)\right\}, \tag{3-25}$$

where

$$h(z_i) = \sqrt{\frac{T_{z_i}^2 - jS(L)(1 + jC_{z_i})}{\pi}} \sum_{l=-N/2}^{N/2} b_l \int_{z_i}^{L} \frac{\exp(-w(y) - a_l(y))}{T(y)\sqrt{T_{z_i}^2 - jS(y)(1 + jC_{z_i})}} \frac{dy}{\sqrt{\delta(L,y)R(y)}}, \tag{3-26}$$

$$R(y) = \frac{1}{T^2(y)} + \frac{1 + jC(y)}{2T^2(y)}, \quad \delta(L,y) = \frac{1 - 2j(S(L) - S(y))R(y)}{R(y)}, \tag{3-27}$$

$$b_l = \begin{cases} 1 & if \quad l = 0 \\ 2 & otherwise \end{cases}, \quad a_l(y) = \left\{\frac{1 + jC(y)}{3 + jC(y)}\frac{1}{T^2(y)} + \frac{4}{(3 + jC(y))\delta(L_{z_i},y)}\right\} \cdot (l \cdot T_b)^2, \tag{3-28}$$

$$\theta(L) = \frac{1}{2}\tan^{-1}\left[\frac{S(L)}{T_{z_i}^2 + C_{z_i}S(L)}\right], \tag{3-29}$$

$$S(y) = \int_{z_i}^{y} \beta_2(s)ds, \quad w(y) = \int_{z_i}^{y} \alpha(s)ds, \tag{3-30}$$

$$T(y) = \frac{\sqrt{(T_{z_i}^2 + C_{z_i}S(y))^2 + S^2(y)}}{T_{z_i}}, \tag{3-31}$$

$$C(y) = \frac{S(y) + C_{z_i}T_{z_i}^2 + C_{z_i}^2S(y)}{T_{z_i}^2}. \tag{3-32}$$

From (3-25), the nonlinear phase shift due to SPM and IXPM is given below:

$$\begin{aligned}\phi_{NL,z_i} &= \tan^{-1}\left\{\frac{\gamma E_{z_i}\,\text{Re}\left[h(z_i)\right]}{1 - \gamma E_{z_i}\,\text{Im}\left[h(z_i)\right]}\right\} \\ &\cong \gamma\,\text{Re}\left[h(z_i)\right]\left\{1 + \gamma E_{z_i}\,\text{Im}\left[h(z_i)\right]\right\}E_{z_i}.\end{aligned} \tag{3-33}$$

Thus the fluctuation of the nonlinear phase is:

$$\delta\phi_{NL,z_i} = \gamma \operatorname{Re}\left[h(z_i)\right]\{1 + 2\gamma E_{z_i} \operatorname{Im}\left[h(z_i)\right]\}\delta E_{z_i}. \tag{3-34}$$

First we consider the nonlinear phase fluctuation caused by the amplifier located at z_i and let δE_{z_i} denotes the energy fluctuation due to ASE noise. Due to SPM and IXPM, energy fluctuations are translated into phase fluctuations. From Eq. (3-34), we see that the nonlinear phase noise has the same statistical properties as the energy fluctuation within the regime of our first-order perturbation theory. As the energy fluctuation is caused by the amplified spontaneous emission noise which is a Gaussian noise, the nonlinear phase noise is a Gaussian process.

From (3-34), we obtain the nonlinear phase fluctuation and the variance of the nonlinear phase noise caused by the amplifier located at z_i:

$$\left\langle \delta\theta_{NL,z_i}^{\;2} \right\rangle = \gamma^2 \operatorname{Re}\left[h(z_i)\right]^2 \cdot \{1 + 2\gamma E_{z_i} \operatorname{Im}\left[h(z_i)\right]\}^2 \left\langle \delta E_{z_i}^{\;2} \right\rangle. \tag{3-35}$$

And the energy fluctuation is given by [2],

$$\left\langle \delta E_{z_i}^{\;2} \right\rangle = 2\rho E_{z_i}, \tag{3-36}$$

where ρ is the ASE power spectral density per polarization given by

$$\rho = n_{sp} hf(G-1). \tag{3-37}$$

Since the noises of amplifiers are statistically independent, the variance of nonlinear phase noise due to all amplifiers $\sigma_{NL}^{\;2}$ is obtained by adding the

37

variance of the nonlinear phase noise caused by each of the amplifiers in the system.

With the assumption that the linear phase noise and the nonlinear phase noise are independent, we can get from Eqs. (3-6) and (3-35) the characteristic function of the addition of linear phase noise and nonlinear phase noise, and thus the p.d.f of the differential phase $\Delta\phi_{L+NL}$ [27]:

$$p(\Delta\phi_{L+NL}) = \frac{1}{2\pi} + \frac{1}{\pi}\sum_{m=1}^{\infty} C_m{}^2 \exp\left[-(2n+1)^2 \sigma_{NL}{}^2\right]\cos(m\Delta\phi_{L+NL}).$$ (3-38)

The expectation of $\cos\left[(2n+1)\Delta\phi_{L+NL}\right]$ in Eq. (3-5) can thus be determined:

$$E\left\{\cos\left[(2n+1)\Delta\phi_{L+NL}\right]\right\} = \int_0^{2\pi}\cos\left[(2n+1)\Delta\phi_{L+NL}\right]\cdot p(\Delta\phi_{L+NL})\cdot d\Delta\phi_{L+NL}$$ (3-39)

$$= \frac{\pi}{4}\rho_s e^{-\rho_s}\left[I_n\left(\frac{\rho_s}{2}\right) + I_{n+1}\left(\frac{\rho_s}{2}\right)\right]^2 \cdot \exp\left[-(2n+1)^2 \sigma_{NL}{}^2\right]$$

3.1.3   Phase Noise Induced by IFWM

The expectation of $\cos\left[(2n+1)\Delta\phi_{IFWM}\right]$ in Eq. (3-5) can be calculated semi-analytically, similar to the approach in [7]. Firstly, we fix the two adjacent central bits to be "1", and let the other bit slots change in order to exhaust all the possible bit patterns. For each bit pattern, the phase shifts of the central two bits induced by IFWM, $\phi_{IFWM}(t)$ and $\phi_{IFWM}(t-T_b)$ are fixed, and can be calculated numerically, thus $\Delta\phi_{IFWM} = \phi_{IFWM}(t) - \phi_{IFWM}(t-T_b)$ calculated at the central two bit slots is a fixed number. For each bit pattern $\{b_n\}$ the error probability can be determined from Eq. (3-5):

$$Pe_{\{b_n\}} = \frac{1}{2} - \frac{\rho_s e^{-\rho_s}}{2} \sum_{n=0}^{\infty} \frac{(-1)^n}{(2n+1)} \left[I_n\left(\frac{\rho_s}{2}\right) + I_{n+1}\left(\frac{\rho_s}{2}\right) \right]^2$$
$$\cdot \exp\left[-(2n+1)^2 \sigma_{NL}^2 \right] \cdot \cos[(2n+1)\Delta\phi_{IFWM}] . \qquad (3\text{-}40)$$

Thus by exhausting all the bit patterns, the error probability of a system based on DPSK including all the three noise sources (IFWM, linear phase noise and nonlinear phase noise) can be given as:

$$Pe_{ALL} = E\left\{ \frac{1}{2} - \frac{\rho_s e^{-\rho_s}}{2} \sum_{n=0}^{\infty} \frac{(-1)^n}{(2n+1)} \left[I_n\left(\frac{\rho_s}{2}\right) + I_{n+1}\left(\frac{\rho_s}{2}\right) \right]^2 \cdot \exp\left[-(2n+1)^2 \sigma_{NL}^2 \right] \cdot \cos[(2n+1)\Delta\phi_{IFWM}] \right\} . \qquad (3\text{-}41)$$

where $E\{\cdot\}$ denotes the ensemble average over all bit patterns. Eq. (3-41) is one of the major expressions we derived in this chapter to calculate the error probability for systems based on DPSK.

3.2   Error Probability for On-off Keying (OOK) Modulation Format

For the long-haul fiber optical communication systems based on OOK modulation format, the p.d.f of the received field using square-law detection was evaluated in [40] for the linear system where the signal is impaired by the Gaussian ASE noise only; and the error probability is evaluated thereafter. While for the nonlinear system, intra-channel nonlinearities such as IXPM and IFWM impair the system greatly [41]. In this section, we use the approach of [40] to calculate the error probability of OOK format with only ASE noise, and then we include the intra-

channel nonlinear effects numerically [6] to obtain the exact error probability for

OOK format.

For the square-law detection, the output is given by:

$$s = |u(t) + n(t)|^2,$$ (3-42)

where $u(t)$ is the complex signal and $n(t)$ is the complex Gaussian noise. The

probability density function of the received signal is given by [40]:

$$f_P(x) = \frac{1}{N_0}\left(\frac{x}{P}\right)^{1/2} \exp\left(-\frac{x+P}{N_0}\right) I_0\left(2\frac{\sqrt{xP}}{N_0}\right) \quad x > 0,$$ (3-43)

where $N_0 / 2$ is the noise variance per dimension, P is the signal power at the

time of detection, I_0 denotes the 0th modified Bessel function of the first kind.

If the receiver threshold is ς, then the probability of error occurs if a "0"

is decided when a "1" is sent, or a "1" is decided when a "0" is sent, thus we have

[40]:

$$p(0\,|\,1) = \int_0^\varsigma f_{P_0}(x)dx = 1 - Q_1\left(\sqrt{\frac{2P_0}{N_0}}, \sqrt{\frac{2\varsigma}{N_0}}\right),$$ (3-44)

$$p(1\,|\,0) = \int_\varsigma^\infty f_0(x)dx = Q_1\left(0, \sqrt{\frac{2\varsigma}{N_0}}\right) = \exp(-\frac{\varsigma}{N_0}).$$ (3-45)

where P_0 is the peak power of signal "1", $Q_1(\cdot,\cdot)$ is the Marcum's Q function of

the first order, and it is defined in [42]:

$$Q_1(\sqrt{a}, \sqrt{b}) = e^{-(a+b)/2} \sum_{k=0}^\infty \left(\frac{a}{b}\right)^{k/2} I_k(\sqrt{ab}).$$ (3-46)

The error probability of OOK format is: $Pe = [p(0|1) + p(1|0)]/2$, and the threshold ς can be solved numerically by searching the optimum value of ς that minimizes Pe.

By considering the intra-channel nonlinear effects, we can write the received signal as

$$s = |u(t) + \delta u + n(t)|^2,$$ (3-47)

where δu is the field due to intra-channel nonlinear effects.

We can get the error probability semi-analytically. First, we fix the central bit of a bit stream to be "1" and let the other bit slots change randomly to exhaust all possible bit patterns, we obtain the field δu_1 due to ghost pulses in the central bit caused by intra-channel nonlinear effects. For each bit pattern, the field due to ghost pulses at the central bit is fixed, and we can view $u(t) + \delta u_1$ as the new signal part.

$$P = |u + \delta u_1|^2 = P_0 \left| 1 + \frac{\delta u_1}{\sqrt{P_0}} \right|^2.$$ (3-48)

We can get the error probability for a single bit pattern $\{b_n\}$:

$$P_{\{b_n\}}(0|1) = 1 - Q_1 \left(\sqrt{\frac{2 P_0 \left| 1 + \frac{\delta u_1}{\sqrt{P_0}} \right|^2}{N_0}}, \sqrt{\frac{2\varsigma}{N_0}} \right).$$ (3-49)

41

As the bit pattern changes, the field due to ghost pulses on the central bit

fluctuates, and the error probability for "1" can be obtained by taking the

ensemble average over all the possible bit patterns, i.e.,

$$p_{NL}(0\,|\,1) = E\left\{1 - Q_1\left(\sqrt{\frac{2P_0\left|1 + \frac{\delta u_1}{\sqrt{P_0}}\right|^2}{N_0}}, \sqrt{\frac{2\varsigma}{N_0}}\right)\right\}.$$
(3-50)

In the same way, we can fix the central bit of the bit stream to be "0", and exhaust

all the bit patterns, we can get the error probability for "0" including intra-channel

nonlinear effects by averaging over all the possible bit patterns:

$$p_{NL}(1\,|\,0) = E\left\{Q_1\left(\sqrt{\frac{2|\delta u_0|^2}{N_0}}, \sqrt{\frac{2\varsigma}{N_0}}\right)\right\},$$
(3-51)

where δu_0 is the field due to ghost pulses caused by intra-channel nonlinear

effects.

Using Eqs. (3-50) and (3-51), we can get the formula of BER for systems

based on OOK format semi-analytically:

$$Pe_{NL} = [p_{NL}(0\,|\,1) + p_{NL}(1\,|\,0)]/2$$
(3-52)

The threshold ς here can be solved numerically by searching the optimum value

of ς that minimizes Pe_{NL}. Eq. (3-52) is another important expression derived in

this chapter to calculate the error probability for systems based on OOK.

3.3   Numerical Simulation for the Error Probability for DPSK and OOK

In this section, the analytical expression for the variance of the ASE induced nonlinear phase noise due to SPM and IXPM is verified by comparing the analytical result with the numerical simulation of the Nonlinear Schrödinger Equation (NLS) using the split-step Fourier method. And then the system performance of the DPSK and OOK are studied using the semi-analytical expression derived in section 3.1 and 3.2.

3.3.1   Verification of the model for the variance of nonlinear phase noise

The schematic of the system used here is shown in Fig. 3-1. The wavelength is 1.55um, computational bandwidth = 24 THz, the optical filter is an ideal band pass filter with full bandwidth of 46 GHz, and the bit rate is 40 Gb/s. Amplifier Spacing is 80 km. The Monte-Carlo Simulation of the nonlinear Schrödinger equation is carried out using the split-step Fourier method with 2000 realizations and the variance of the nonlinear phase noise is calculated similar to the way in [5].

If the residual dispersion between amplifiers is zero, the effects of inter-channel XPM and FWM are enhanced due to resonance [43]. In Ref. [41], it was shown that, intra-channel nonlinear effects are also enhanced in such a dispersion map, and this map is called the resonant map. In this subsection, we compare the impact of nonlinear phase noise in resonant and non-resonant dispersion maps.

Firstly we use a resonant dispersion map to verify the analytical variance of the nonlinear phase noise derived in section 3.1.2, which is to say, $D_1 + D_2 = 0$, and no pre- and post- compensation fibers are used. In Fig.3-2, we verify the analytical variance of the ASE induced nonlinear phase noise due to SPM alone, using a single Gaussian pulse with 8.33 ps pulse width (FWHM) and 2 mW peak power. The solid line and dotted line in Fig.3-2 show the numerical simulation and analytical results, respectively. We can see from Fig.3-2 that they match very well. In addition, we see from Fig.3-2 that, when the dispersion becomes larger, the ASE induced nonlinear phase noise due to SPM becomes quite small and the linear phase noise is dominant.
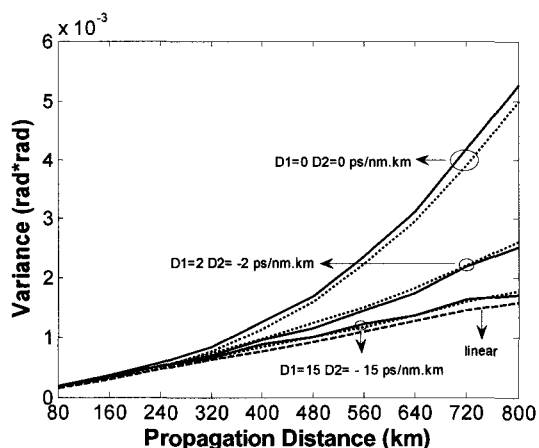
Fig. 3-2 Variance of phase noise for a single pulse. Solid Line and dotted line show the numerical and analytical results, respectively. The dashed line shows variance of linear phase noise by letting the nonlinear coefficient to be zero in the simulation.

44

Below in Fig.3-3, we verify the model for ASE induced nonlinear phase noise due to SPM and IXPM by using 17 pulses. We fix the central pulse to be bit '1', whereas all the other bits are changed randomly in the Monte-Carlo Simulation with 2000 realizations. The width (FWHM) is 8.33 ps, and the separation between each two pulses is 25 ps. Here we use two dispersion maps: 1) D1 = D2 = 0 ps/nm.km; 2) D1 = 15.0 ps/nm.km, D2 = -15.0 ps/nm.km. All the other parameters are the same as above. The solid line and dotted line show the numerical simulation result and analytical result for the phase noise including linear phase noise and ASE induced nonlinear phase noise due to SPM and IXPM. In order to get the numerical result for the phase noise including only the linear and nonlinear phase noise, we have subtracted the phase noise induced by IFWM (by setting $n_{sp} = 0$) from the total numerical phase noise when $n_{sp} = 1$. Comparing Fig.3-2 and Fig.3-3, we see that, when the dispersion is small, the ASE induced nonlinear phase noise due to SPM is dominant; however, as the dispersion increases, the effect of ASE induced nonlinear phase noise due to IXPM becomes more dominant. This is because as dispersion increases, the pulse in the central bit slot interacts nonlinearly with many neighboring pulses due to pulse spreading.

In Fig. 3-4, we use the resonant map and show the phase variance of IFWM, and that of the ASE induced nonlinear phase noise due to SPM and IXPM as a function of fiber dispersion coefficient $D = |D_1| = |D_2|$. The phase variance of IFWM is: $\sigma^2{}_{IFWM} = \langle \phi^2 \rangle - \langle \phi \rangle^2$, where ϕ is the change in phase of the central

pulse at t=0 due to IFWM. We set n_{sp} =0 in the simulation, and fix the central

pulse to be bit '1' and exhaust all the possible bit patterns and calculate the

variance of the peak phase of the central pulse. The dependence of IFWM and

nonlinear phase noise on dispersion is similar to that observed in [44].
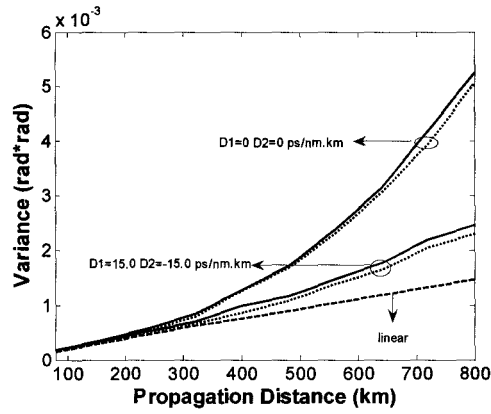
Fig.3-3 Variance of phase noise including the effects of SPM and IXPM. Solid line and dotted line

show the numerical and analytical results of the phase noise, respectively. Dashed line shows the

linear phase noise only.
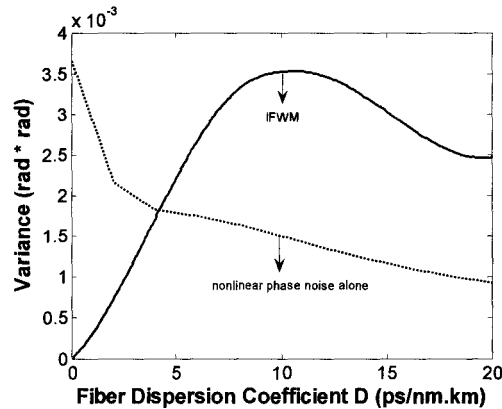
Fig. 3-4 Variance of the phase noise due to IFWM alone, and due to the nonlinear phase noise

including the effects of SPM and IXPM for the resonant dispersion map.

Next, we verify the analytical expression of the nonlinear phase noise in a non-resonant dispersion- managed system with equal pre- and post- compensation fibers. In Fig. 3-5, we use two dispersion maps: 1) D1 = 3.0 ps/nm.km, D2 = -0.5 ps/nm.km; 2) D1 = 17.0 ps/nm.km, D2 = -14.5 ps/nm.km. For both dispersion maps, the residual accumulated dispersion within an amplifier spacing is 100 ps/nm.
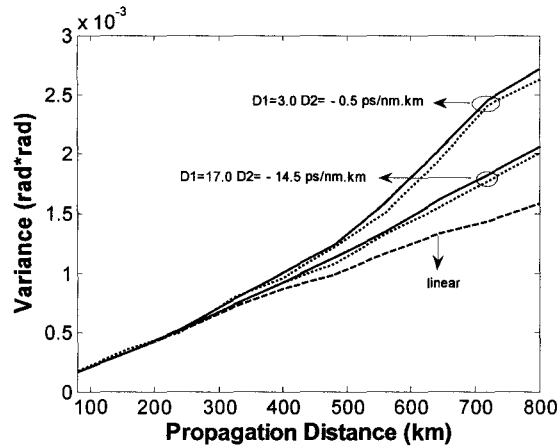
Fig. 3-5 Variance of phase noise including the effects of SPM and IXPM for a non-resonant dispersion map. Solid line and dotted line show the numerical and analytical results of the phase noise, respectively. Dashed line shows the linear phase noise obtained by setting the nonlinear coefficient to zero in the simulation.

In Fig.3-6, we use the same non-resonant dispersion-managed map as above, and show the comparison of variance of the phase noise induced by IFWM alone and the ASE induced nonlinear phase noise due to SPM and IXPM, as functions of the dispersion coefficient of the anomalous fiber $D = D_1$,

while $D_2 = -|D_1| + 2.5$ ps/nm.km. In this non-resonant map, we see that the variance

of the nonlinear phase noise is reduced as compared to the resonant map. In

contrast to the results in Ref. [44], the phase variance of IFWM noise is larger

than that of the nonlinear phase noise in our case. This is probably because in Ref.

[44] only one type of transmission fiber is used, whereas in our system we use the

dispersion managed fibers with pre- and post- compensation fibers. Intra-channel

nonlinear impairments are sensitive to dispersion maps since the efficiency of

ghost pulse generation due to IFWM depends on the degree of overlap between

signal pulses during propagation due to dispersion broadening [41].
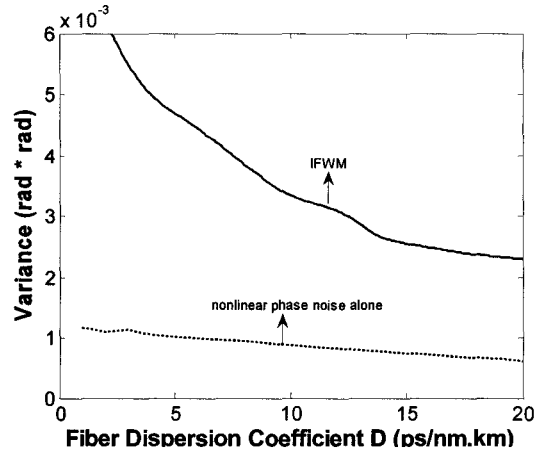
Fig.3-6 Variance of the phase noise due to IFWM and the nonlinear phase noise for a non-resonant dispersion-managed system. (D=D1, D2= -D1 +2.5 ps/nm.km).

3.3.2 Numerical Simulation for Systems based on DPSK

In the system here, we use the following parameters throughout the paper unless

otherwise specified: the bit rate is 40 Gb/s, pulse width (full width at half-

maximum) is 8.33 ps, and the average launch power is 1 mW. The structure of the system is the same as in Fig. 3-1. The other parameters are as follows: $D1 = 17.0$ ps/nm.km, $D2 = -14.5$ ps/nm.km, $\gamma_1 = 2.5$ $W^{-1} km^{-1}$, $\gamma_2 = 10$ $W^{-1} km^{-1}$, $\alpha_1 = \alpha_2 = 0.2$ dB/km, $D_{pre} = D_{post} = -100$ ps/nm.km, $\alpha_{pre} = \alpha_{post} = 0.5$ dB/km. The total transmission distance is 800 km, excluding pre- and post-compensation fibers.

Here we calculate the BER semi-analytically using Eq. (3-41). To calculate $E\{\cos[(2n+1)\Delta\phi_{IFWM}\}$, we have carried out the numerical simulation of the nonlinear Schrödinger equation using a 16-bit sequence. We treat the phase of each bit at the transmitter as a discrete random variable taking a value "0" or "π", and fix the central two bit slots to be "1" (or zero phase). For each bit pattern, $\Delta\varphi_{IFWM}$ is calculated, and BER is evaluated using Eq. (3-41), with the variance of nonlinear phase noise obtained analytically from the expression in Section 3.1.2. In the simulation, ASE noise has been excluded so that the noises at the central two bits are caused solely by IFWM. The numerical simulation has been carried out using a split-step Fourier scheme with a simulation bandwidth of 24 THz.

We calculate the differential phase shift in the central of the bits due to IFWM using the following formulae:

$$\Delta\phi_{IFWM} = \phi_{IFWM\ 0} - \phi_{IFWM\ 1}, \tag{3-53}$$

where $\phi_{IFWMj} = \sin^{-1}\left(\frac{Im(u_j)}{|u_j|}\right)$, $j = 0, 1$. u_0 and u_1 are the complex received fields at the middle of the central two bit slots.

49

Fig. 3-7 shows the dependence of error probability (BER) on pre-compensation length for DPSK format. The total length of pre- and post-compensation fibers is fixed to be 10 km, so that the accumulated dispersion at the receiver end will be zero. From Fig. 3-7, we see that the optimum pre-compensation fiber length is 5.5 km, which corresponds to a pre-compensation of -550 ps/nm. By optimizing the pre- compensation length, the impact of IFWM can be minimized. Also, our results show that, the optimum pre-compensation length is independent of the launch power. In all the simulation below for systems based on DPSK, we choose the pre-compensation fiber length to be 5.5 km.

3.3.3 Numerical Simulation for Systems based on OOK

For the OOK format, we use the same parameters as in section 3.3.2. Fig. 3-8 shows the dependence of BER on the pre- compensation length for OOK format. The average launch power in Fig. 3-8 is 1 mW. First we fix the central bit to be '1', and exhaust the bit patterns to calculate $p_{NL}(0|1)$ from Eq. (3-50). We then repeat the process by fixing the central bit to be '0' and calculate the BER using Eq. (3-51). From Fig.3-8, we see that the optimum pre-compensation fiber length is 8.0 km, and this length is independent of the launch power for systems based on OOK. From Fig.3-7 and Fig.3-8, we see that optimizing the pre-compensation length in both OOK and DPSK can lead to significant performance improvement.
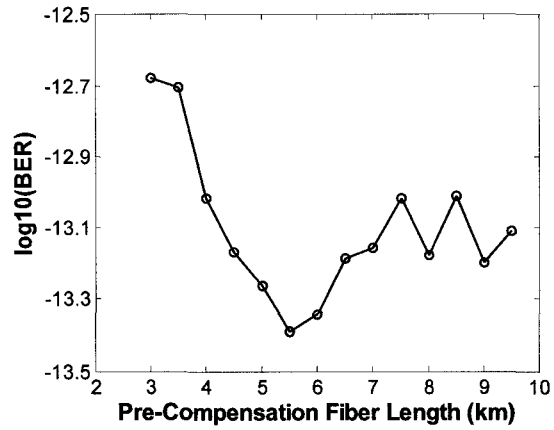
Fig. 3-7 Dependence of BER on pre-compensation length for systems based on DPSK

(SNR=15dB).
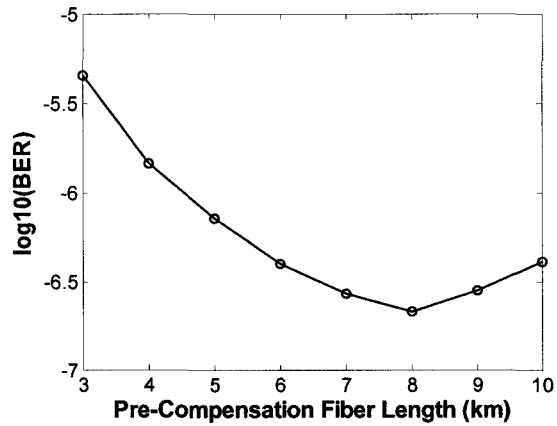
Fig. 3-8 Dependence of BER on pre-compensation length for systems based on OOK

(SNR=15dB).

3.3.4   Comparison between DPSK and OOK Formats

Fig. 3-9 shows the comparison of the error probability as a function of SNR for

systems based on DPSK and OOK considering only the linear amplified

spontaneous emission noise.
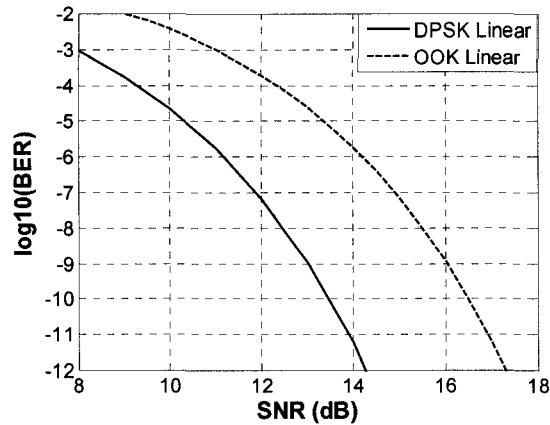
Fig. 3-9 Dependence of BER on SNR for systems based on DPSK and OOK in the absence of
nonlinearity.

From Fig. 3-9, we see that in a linear system, to arrive the BER of 10^{-9}, the

difference in SNR between systems based on DPSK and OOK is 3 dB, which is

consistent with the linear theory [2]. However for a nonlinear system, since the

effects of nonlinearity on systems based on DPSK and OOK are different, the

difference of SNR should exceed 3 dB to reach the given BER of 10^{-9}, which can

be determined from Eqs. (3-41) and (3-52). Fig. 3-10 shows the required SNR for

these two systems to reach the BER of 10^{-9} for different launch powers. The solid

line with 'x' and the solid line with diamond are the required SNR for non-

resonant dispersion-managed systems based on DPSK and OOK under different launch powers in order to reach the given BER of 10^{-9}, respectively. From Fig. 3-10, we see that for the launch powers below -3 dBm, the difference in SNR between systems based on DPSK and OOK to reach this given BER is around 3 dB. When the launch power is 0 dBm, the SNR difference is 6 dB, and this difference increases as the launch power increases. During the simulation, the pre-compensation fiber lengths of the two systems are optimized. The duty-cycle of OOK and DPSK formats is 33%, and the root-mean-square (RMS) spectral width of both formats is the same for each given launch power. We have also shown the SNR required to reach the given BER under different launch power for the resonant dispersion map with D1= 17 ps/nm.km, D2= - 17 ps/nm.km. The dotted line with 'x' and the dotted line with diamond in Fig. 3-10 are the required SNR for resonant systems based on DPSK and OOK for different launch powers in order to reach the given BER of 10^{-9}, respectively. Comparing the results of resonant and non-resonant dispersion-managed maps in Fig.3-10, we see that there is a significant improvement in performance for both formats if non-resonant dispersion map is used.

Fig. 3-11 shows the required SNR as a function of launch power to attain a specific BER. For the given power spectral density of ASE and for the given system configuration, SNR can be calculated as a function of launch power. Using

Fig. 3-11, the optimum launch power (if it exists) for that SNR to reach a specific

BER can be calculated.
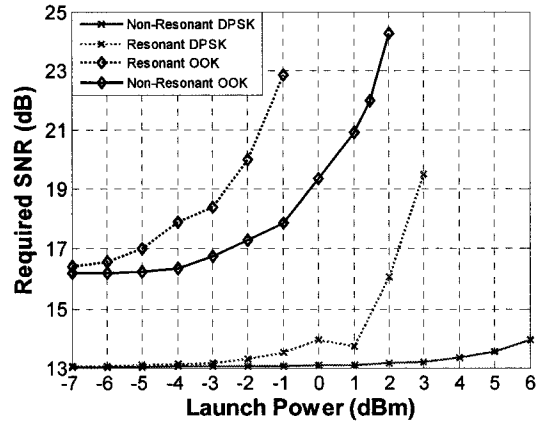
Fig. 3-10 Dependence of SNR on the launch power to reach the given BER of 10^{-9}. The solid line

with 'x' and the solid line with diamond show the required SNR for non-resonant dispersion-

managed systems based on DPSK and OOK for different launch powers, respectively. The dotted

line with 'x' and the dotted line with diamond show the required SNR for resonant dispersion-

managed systems based on DPSK and OOK for different launch powers, respectively.
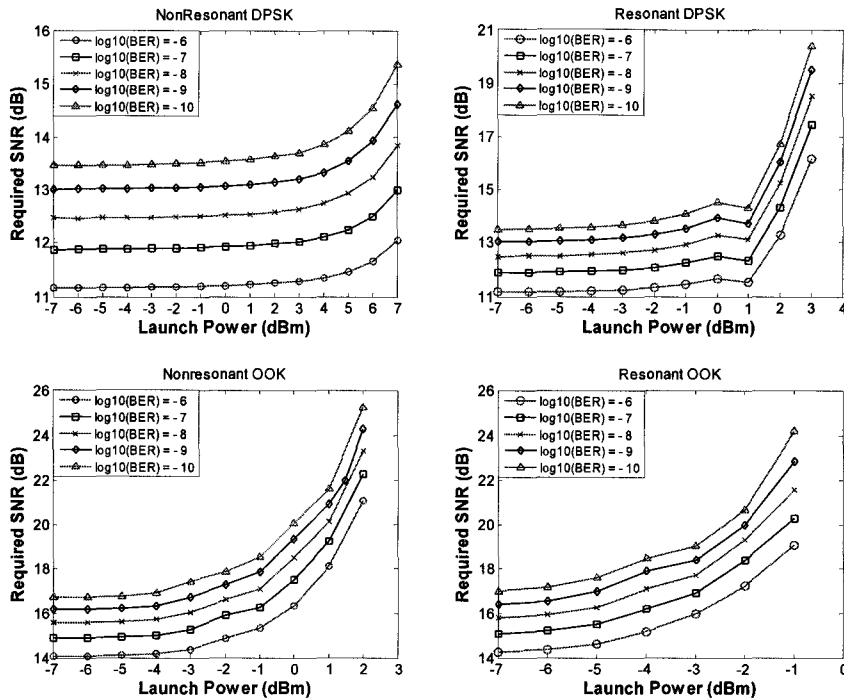
Fig. 3-11 The Required SNR to reach the given BER of $10^{-6}, 10^{-7}, 10^{-8}, 10^{-9}$ and 10^{-10} for different launch power for various systems examined in our paper (non-resonant DPSK, resonant DPSK, non-resonant OOK and resonant OOK), respectively.

3.4   Concluding Remarks

In summary, we have derived an analytical expression for the variance of ASE induced nonlinear phase noise including the effects of SPM and IXPM in dispersion-managed transmission systems, and validated this expression by numerical simulation of the nonlinear Schrödinger equation. We have also developed semi-analytical expressions for the error probability for systems based on DPSK and OOK. The optimum pre-compensation lengths for DPSK and OOK

formats are calculated and it is shown that optimizing the pre-compensation length for both DPSK and OOK formats can both improve the performance. Under the optimized conditions, the performance of DPSK and OOK formats in our system is studied and compared for different launch powers. Our results show that to achieve the given BER of 10^{-9}, the difference in SNR between systems based on DPSK and OOK is around 3 dB when the launch power is small in agreement with the linear theory. However, as the launch power increases, the SNR difference increases implying that a system based on DPSK is more tolerant to nonlinear impairments than OOK. We have compared the performance of a system using resonant and non-resonant dispersion maps, and results show that the performance can be significantly improved for both formats if the non-resonant dispersion map is used.

4

Rayleigh Backscattering in Single-Source Bidirectional FTTH Passive Optical Networks Using Different Modulation formats

The network size and connection complexity of a fiber-to-the-home (FTTH) passive optical network (PON) can be reduced by using bidirectional transmission in a single fiber [8, 45-47]. Hall et al [45] first demonstrated the feasibility of such a network. Currently in a PON, different laser sources with separate wavelengths are used for the downstream and upstream transmission in Optical Line Terminal (OLT) and Optical Network Unit (ONU) [46]. However, if a reflective modulator is implemented in ONU, the laser source in ONU is avoided, preventing its stabilization [8, 47]. In addition, the single-source topology makes the ONU

wavelength independent and thus convenient for wavelength-division multiplexing (WDM) operation.

Different modulation formats have been recently proposed and demonstrated for the single-source structure. In Ref. [9], it is shown that the bidirectional transmission using on-off keying (OOK) for both downstream and upstream is feasible. In Ref. [10] a topology known as frequency-shift keying (FSK)/OOK in which FSK for downstream and OOK for upstream is presented. However, because of the incoherent FSK receiver, the signal bandwidth is larger than that required by OOK or differential phase-shift keying (DPSK). In addition, DPSK format has the well-known advantage of 3dB signal-to-noise ratio (SNR) over FSK and OOK to reach the given bit error ratio (BER) [2, 48]. Therefore, in this chapter we analyze the error probability of a system based on DPSK/OOK topology and compare it with that of a system based on OOK/OOK topology.

For the single-source bidirectional system, Rayleigh Backscattering noise has been viewed as one of the most dominant noise sources. Rayleigh backscattering noise has been studied extensively both analytically and experimentally for a system based on on-off keying (OOK) [36-37, 49-50]. In Ref. [49], an expression for the error probability of a system based on OOK taking into account the Rayleigh backscattering field is derived. However, the power spectral density (PSD) of the OOK signal is not included in their derivation. In this section, an analytical expression for the probability density function (pdf) of the

Rayleigh backscattering field caused by OOK signal is derived without ignoring

the PSD of the OOK signal, and the error probability for bidirectional systems

using OOK/OOK topology is derived. The properties of Rayleigh backscattering

field caused by DPSK signal have also been evaluated, and the error probabilities

for bidirectional systems using DPSK/OOK topology have been estimated. To the

best of our knowledge, this has not been done before. Our results show that, to

acquire the given error probability (BER) of 10^{-9}, the required receiver power in

bidirectional optical systems using DPSK/OOK topology is around 9 dBm lower

than that in the system using OOK/OOK topology if non-return-to-zero (NRZ)

signal is used. We have also studied the effect of duty cycle on the system

performance, and our results show that, for both OOK/OOK topology and

DPSK/OOK topology, using return-to-zero (RZ) signal can lead to significant

performance improvement compared with the non return-to-zero (NRZ) signal,

however, the corresponding improvement in a system based on OOK/OOK

topology is larger than that of a system based on DPSK/OOK topology.

In Section 4.1 we give the detailed structure of the bidirectional systems

using OOK/OOK topology and DPSK/OOK topology. Section 4.2 examines the

statistical properties of Rayleigh backscattering field caused by DPSK signal and

OOK signal. The analytical expressions for the error probabilities in systems using

OOK/OOK and DPSK/OOK topologies have been derived in Section 4.3. Section

4.4 gives the simulation results, and Section 4.5 summarizes our results.

4.1   Network structure

Use of the single-source bidirectional system in FTTH networks not only

simplifies the system structure, but also makes it possible to transit the current

time-division multiplexing (TDM) scenario to the wavelength-division

multiplexing (WDM) structure, as the ONUs are now wavelength independent

[9]. A bidirectional OOK/OOK structure was implemented and proved feasible in

Ref. [9] at the bit rate of 1.25 Gb/s. The structure of the OOK/OOK topology is

shown in Fig. 4-1. To simplify the structure, single OLT and ONU are displayed

in the structure. For multiple OLTs and ONUs, an arrayed waveguide grating

(AWG) can be used to wavelength-multiplex the optical signals into the fiber. A

reflective semiconductor optical amplifier (RSOA) is used in the ONU acting as

modulator and photo-detector, and an interface circuit is used to separate the

received downstream and upstream data for RSOA. The bias current determines

whether the RSOA is working as a modulator or detector. An optical circulator is

used in OLT to direct the upstream signal to the detection circuit. As the intensity

modulated signal (on-off keying) does not contain the carrier information needed

for the upstream transmission, burst-mode transmission was used in Ref. [9].

Downstream data and upstream carrier are sent from the OLT time multiplexed in a single burst, as shown in Fig. 4-1.

Next let us consider the FSK/OOK topology. Since the intensity of the downstream FSK signal is constant, the direct intensity modulation of the signal at ONU is possible which simplifies the transmission protocol. Thus unlike the OOK/OOK topology, it is not required to send the downstream carrier for FSK/OOK topology. In Ref. [10] an access topology based on FSK downstream and OOK upstream has been presented at a bit rate of 1 Gb/s transmitted up to 30 km in single-mode fibers. At the ONU, an FSK optical detector to decode downstream data and an intensity modulator to encode upstream data are used.

Another attractive alternative is to use DPSK for downstream and OOK for upstream. As the DPSK signal is constant in power, it allows the direct remodulation for the OOK upstream data, without requiring the upstream carrier from the OLT. In addition, as the detection of DPSK signal only depends on the relative phase between the two successive bits, by using DPSK balanced receiver, the downstream data can be demodulated without needing a synchronous carrier. Fig. 4-2 shows the system structure using the DPSK for downstream signal and OOK for upstream signal transmission. In OLT, the continuous wave from the DFB laser is externally phase-modulated by the Mach-Zehnder Modulator (MZM). While in ONU, an optical circulator is used to separate the downstream and upstream data. To detect the downstream data, a DPSK balanced receiver [2]

consisting of a delay-interferometer (DI) and two photodiodes is used. The downstream signal which is constant in intensity is remodulated by the upstream OOK signal using RSOA as shown in Fig. 4-2. In the following section, we examine and compare the system performance of OOK/OOK and DPSK/OOK topologies.
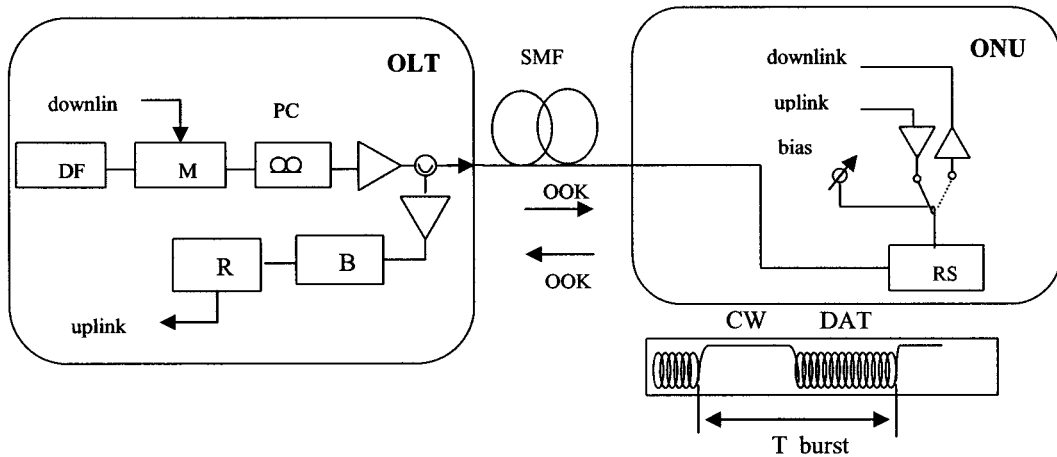
Fig. 4-1 Schematic of OOK/OOK modulation for downstream and upstream data in FTTH
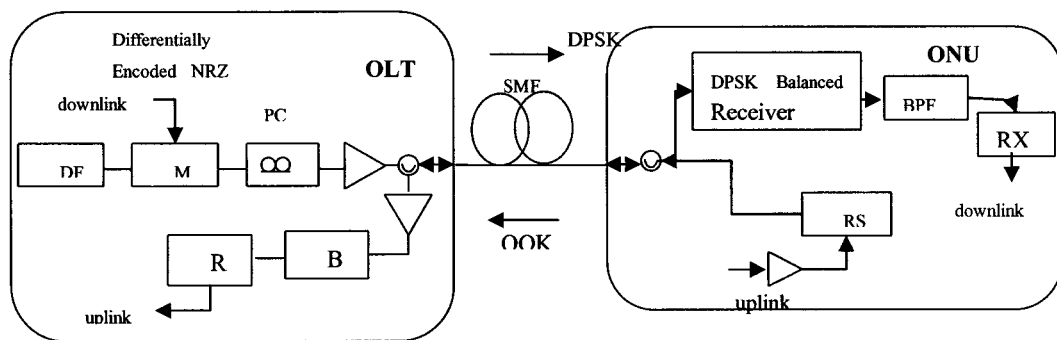
Fig.4- 2 Schematic of DPSK/OOK modulation for downstream and upstream data in FTTH

4.2 Rayleigh Backscattering caused by DPSK Signal and ook signal

4.2.1 Rayleigh Backscattering Caused by DPSK Signal

In this subsection, we will study the statistical properties of Rayleigh backscattering field caused by the DPSK signal. The power spectral density (PSD) of this noise field is needed for calculating the error probability in OLT of the system using DPSK/OOK topology when this noise field interacts with the upstream OOK signal. The field of Rayleigh Backscattering noise $\varepsilon_{b-DPSK}(t)$ is related to the transmitted source $\varepsilon_{s-DPSK}(t)$ in the following model [36]:

$$\varepsilon_{b-DPSK}(t) = \int_0^L \varepsilon_{s-DPSK}(t - \frac{2z}{\upsilon})e^{-\alpha z}e^{-j2\beta z}\rho(z)dz, \qquad (4-1)$$

where $\varepsilon_{s-DPSK}(t)$ is the source field which is externally phase modulated, α is the intensity loss coefficient, β is the propagation constant, υ is the velocity of light in the fiber, L is the fiber length. $\rho(z)$ is the backscattering coefficient, and is modeled as a delta correlated circular complex Gaussian (ccG) random variable [36]:

$$\langle \rho^*(z_1)\rho(z_2) \rangle = \alpha_s S\delta(z_1 - z_2), \qquad (4-2)$$

where S and α_s are the recapture factor and the intensity coefficients due to Rayleigh scattering, respectively. Here we assume the polarization state of the

light is preserved along the fiber, which corresponds to the degree of polarization

$P = 1$ in Ref. [49]. The auto-correlation function of the Rayleigh backscattering

field is expressed in terms of the source field as [37]:

$$R_{\varepsilon_{b-DPSK}}(t, t+\tau) = \frac{\alpha_s S \upsilon}{2} \int_0^{T_L} \left\langle \varepsilon^*_{s-DPSK}(t-\tau_1) \varepsilon_{s-DPSK}(t+\tau-\tau_1) \right\rangle e^{-\alpha\upsilon\tau_1} d\tau_1, \qquad (4\text{-}3)$$

where $\tau_1 = 2z/\upsilon$, and $T_L = 2L/\upsilon$ is the fiber round-trip time delay.

For high-speed digital communication systems, typically, the bit interval

T_b is much smaller than the round-trip time delay T_L, and the effective life

time $1/\alpha\upsilon$. Under these conditions, the backscattered field becomes wide-sense

stationary [37]. The time-averaged auto-correlation function of the Rayleigh

backscattering field can be written as:

$$R_{\varepsilon_{b-DPSK}}(\tau) = \frac{\alpha_s S \upsilon}{2} \overline{\left(\frac{1}{T_L} \int_0^{T_L} \left\langle \varepsilon^*_{s-DPSK}(t-\tau_1) \varepsilon_{s-DPSK}(t+\tau-\tau_1) \right\rangle d\tau_1 \right)} \overline{\left(\int_0^{T_L} e^{-\alpha\upsilon\tau_1} d\tau_1 \right)} = B \cdot R_{\varepsilon_{s-DPSK}}(\tau), \qquad (4\text{-}4)$$

where $B = \dfrac{\alpha_s S\left(1 - e^{-2\alpha L}\right)}{2\alpha}$. $\qquad (4\text{-}5)$

The PSD of Rayleigh backscattering field is the Fourier Transform of the auto-

correlation function:

$$S_{\varepsilon_{b-DPSK}}(f) = B S_{\varepsilon_{s-DPSK}}(f). \qquad (4\text{-}6)$$

When the source is externally phase-modulated, the source field can be expressed

as [37]:

$$\varepsilon_{s-DPSK}(t) = \sqrt{P_s}\,\gamma(t)\exp\left[j\left(\omega_0 t - \phi(t)\right)\right], \qquad (4\text{-}7)$$

where $\sqrt{P_s}$ is the source amplitude, ω_0 is the carrier frequency, $\phi(t)$ describes the inherent laser phase noise, and $\gamma(t)$ describes the field envelope. For NRZ-DPSK modulation, $\gamma(t)$ is a non-stationary random process with period T_b and value "+1" and "-1" in equal probability, while for RZ-DPSK with duty cycle d_{cy}, $\gamma(t)$ is a non-stationary process with value "+1" and "-1" in the range $d_{cy}T_b$ with period T_b. The average power of all the systems considered below is kept constant as $P_{av} = P_s d_{cy}$.

Since the laser phase noise $\phi(t)$ and the modulation signal $\gamma(t)$ are statistically independent, the time averaged auto-correlation function of the source field can be expressed as:

$$\begin{aligned}
R_{\varepsilon_{s-DPSK}}(\tau) &= P_s \overline{\langle \gamma^*(t)\gamma(t+\tau) \rangle} \cdot \overline{\langle \exp[j(\phi(t+\tau) - \phi(t))] \rangle} \\
&= P_s R_\gamma(\tau) \cdot R_\phi(\tau)
\end{aligned} \qquad (4\text{-}8)$$

where $R_\gamma(\tau) = \overline{\langle \gamma^*(t)\gamma(t+\tau) \rangle}$, and $R_\phi(\tau) = \overline{\langle \exp[j(\phi(t+\tau) - \phi(t))] \rangle}$. The PSD of the source field is the Fourier Transform of its auto-correlation function. Therefore, we have

$$S_{\varepsilon_{s-DPSK}}(f) = P_s S_\gamma(f) \otimes S_\phi(f), \qquad (4\text{-}9)$$

where $S_\gamma(f)$ and $S_\phi(f)$ are the Fourier Transform of $R_\gamma(\tau)$ and $R_\gamma(\tau)$, respectively, and $\otimes$ denotes the convolution.

Using the statistical model of the laser phase noise in Ref. [51], we have:

$$R_\phi(\tau) = \langle \exp\{j[\phi(t+\tau) - \phi(t)]\} \rangle = \exp(-\pi \Delta f \cdot |\tau|), \qquad (4\text{-}10)$$

where Δf is the laser linewidth, and the corresponding PSD has a Lorenzian shape

given by:

$$S_\phi(f) = \int_{-\infty}^{\infty} R_\phi(\tau)e^{-j2\pi f\tau}d\tau = \frac{2}{\pi}\cdot\frac{\Delta f}{\Delta f^2 + 4f^2}, \quad \Delta f \neq 0 \tag{4-11}$$

The non-stationary modulation signal $\gamma(t)$ can be written as:

$$\gamma(t) = \sum_{n=-N/2}^{N/2} a_n h(t - nT_s), \tag{4-12}$$

where a_n is a random variable with values "+ 1" and "- 1" with equal probability,

N+1 is the total number of bits, and $h(t)$ is the rectangular pulse given by:

$$h(t) = \begin{cases} 1 & if \quad |t| < d_{cy}T_s, \\ 0 & otherwise \end{cases} \tag{4-13}$$

where d_{cy} is the duty-cycle.

Taking Fourier Transform of Eq. (4-12), we get:

$$\gamma(f) = \sum_{n=-N/2}^{N/2} a_n \widetilde{H}(f)e^{-jn2\pi fT_s} \tag{4-14}$$

$$\left\langle |\gamma(f)|^2 \right\rangle = \sum_n \sum_m \left\langle a_n a_m \right\rangle \left\langle e^{-j(n-m)2\pi fT_s} \right\rangle |\widetilde{H}(f)|^2$$

$$= Nd_{cy}^2 T_s^2 \left(\frac{\sin(\pi f d_{cy}T_s)}{\pi f d_{cy}T_s} \right)^2 \tag{4-15}$$

Thus the PSD of the modulation signal is:

$$S_\gamma(f) = \lim_{N\to\infty} \frac{\left\langle |\gamma(f)|^2 \right\rangle}{NT_s} = d_{cy}^2 T_s \left(\frac{\sin(\pi f d_{cy}T_s)}{\pi f d_{cy}T_s} \right)^2. \tag{4-16}$$

66

With the relation $P_{av} = P_s d_{cy}$, we have the PSD of the source field:

$$S_{\varepsilon_s}(f) = P_{av}\left(\frac{2}{\pi} \cdot \frac{\Delta f}{\Delta f^2 + 4f^2}\right) \otimes d_{cy}T_s\left(\frac{\sin(\pi f T_s \cdot d_{cy})}{\pi f T_s \cdot d_{cy}}\right)^2 \qquad (4\text{-}17)$$

and the PSD of the Rayleigh backscattering field caused by DPSK signal is:

$$S_{\varepsilon_{b-DPSK}}(f) = B S_{\varepsilon_{s-DPSK}}(f). \qquad (4\text{-}18)$$

4.2.2   Rayleigh Backscattering Caused by OOK Signal

In this subsection, we study the statistical properties of the Rayleigh backscattering field caused by the OOK signal. The PSD of this noise field is needed to calculate the error probability of the system using OOK/OOK topology in which the Rayleigh backscattering field caused by the downstream (upstream) OOK signal interacts with the upstream (downstream) OOK signal, and also in the ONU of the system based on DPSK/OOK topology in which the Rayleigh backscattering field caused by OOK interacts with the downstream DPSK signal. For the single-source bidirectional system using OOK format, the modulating signal is:

$$\gamma(t) = \sum_{n=-N/2}^{N/2} a_n h(t - nT_s), \qquad (4\text{-}19)$$

where a_n is a random variable with value "0" and "1" in equal probability. The average power is related to the peak power as $P_{av} = P_s d_{cy} / 2$. Define a new random variable b_n:

$$b_n = a_n - 1/2, \tag{4-20}$$

where b_n is a random variable with values "-1/2" and "1/2", and $\langle b_n \rangle = 0$. Thus the non-stationary modulation signal $\gamma(t)$ for OOK can be written as:

$$\gamma(t) = \sum_{n=-N/2}^{N/2} b_n h(t - nT_s) + \frac{1}{2} \sum_{n=-N/2}^{N/2} h(t - nT_s) \tag{4-21}$$

Take the Fourier transform of Eq. (4-21), we get:

$$\gamma(f) = \sum_{n=-N/2}^{N/2} b_n \widetilde{H}(f) e^{-jn2\pi fT_s} + \frac{1}{2} \sum_{n=-N/2}^{N/2} \widetilde{H}(f) e^{-jn2\pi fT_s} \tag{4-22}$$

The PSD of the modulation part is:

$$
\begin{aligned}
S_\gamma(f) &= \lim_{N\to\infty} \frac{\langle |\gamma(f)|^2 \rangle}{NT_s} \\
&= \lim_{N\to\infty} \frac{1}{NT_s} \left(\sum_n \sum_m \langle b_n b_m \rangle e^{-j(n-m)2\pi fT_s} |\widetilde{H}(f)|^2 + \frac{1}{4} \sum_n \sum_m e^{-j(n-m)2\pi fT_s} |\widetilde{H}(f)|^2 \right) \\
&= \lim_{N\to\infty} \frac{1}{NT_s} \left(\frac{1}{4} N |\widetilde{H}(f)|^2 + \frac{1}{4} |\widetilde{H}(f)|^2 \sum_m \left(\sum_n e^{-jn2\pi fT_s} \cdot e^{jm2\pi fT_s} \right) \right)
\end{aligned}
\tag{4-23}
$$

To evaluated Eq. (4-23), we first consider the discrete Fourier transform of $x(n) = 1$ [48]:

$$X(k) = \frac{1}{N} \sum_n 1 \cdot e^{-jk\frac{2\pi}{N}n} = \sum_l \delta(k - lN), \tag{4-24}$$

where $\delta(k - lN)$ is the discrete delta-function with value "1" at the desired point

$k = lN$, and "0" elsewhere. From Eq. (4-24), we have:

$$\sum_n e^{-jn2\pi fT_s} = N\sum_l \delta(NfT_s - lN) = \frac{1}{T_s}\sum_l \delta(f - \frac{l}{T_s})$$

(4-25)

$$\sum_m \left(\sum_n e^{-jn2\pi fT_s} \cdot e^{jm2\pi fT_s}\right) = \sum_m \left(\frac{1}{T_s}\sum_l \delta(f - \frac{l}{T_s}) \cdot e^{jm2\pi fT_s}\right)$$

$$= \frac{N}{T_s}\sum_l \delta(f - \frac{l}{T_s})$$

(4-26)

Insert Eq. (4-26) into (4-23), we have:

$$S_\gamma(f) = \lim_{N\to\infty}\frac{1}{NT_s}\left(\frac{1}{4}N\left|\tilde{H}(f)\right|^2 + \frac{1}{4}\left|\tilde{H}(f)\right|^2\frac{N}{T_s}\sum_l \delta(f - \frac{l}{T_s})\right)$$

$$= \frac{d_{cy}^2}{4}\left(\frac{\sin(\pi fT_s d_{cy})}{\pi fT_s d_{cy}}\right)^2\left(T_s + \sum_n \delta\left(f - \frac{n}{T_s}\right)\right)$$

(4-27)

Thus for the source field described as $\varepsilon_{s-OOK}(t) = \sqrt{P_s}\gamma(t)\exp[j(\omega_0 t - \phi(t))]$, the

PSD of the source field using OOK modulation format is:

$$S_{\varepsilon_{s-OOK}}(f) = \left\{\frac{2}{\pi}\cdot\frac{\Delta f}{\Delta f^2 + 4f^2}\right\} \otimes \left\{\frac{P_{av}d_{cy}}{2}\left(\frac{\sin(\pi fT_s d_{cy})}{\pi fT_s d_{cy}}\right)^2\left[T_s + \sum_n \delta\left(f - \frac{n}{T_s}\right)\right]\right\}.$$

(4-28)

From Eqs. (4-28) and (4-5), the PSD of the RB field is:

$$S_{\varepsilon_{b-OOK}}(f) = BS_{\varepsilon_{s-OOK}}(f).$$

(4-29)

4.3 error probability for systems using OOK/OOK and DPSK/OOK topology

4.3.1 Error Probability for Bidirectional Optical Systems Using OOK/OOK Topology

In both the OLT and ONU of the systems using OOK/OOK topology, the Rayleigh backscattering field caused by the downstream (upstream) OOK signal interacts with the upstream (downstream) OOK signal, leading to performance degradation. Here we consider the error probability in the OLT of the bidirectional system using OOK/OOK topology. The total field $\varepsilon_t(t)$ before the receiver front is the sum of the reflected signal $\varepsilon_r(t)$ and the RB field $\varepsilon_b(t)$, i.e.,

$$\varepsilon_t(t) = \varepsilon_r(t) + \varepsilon_b(t). \tag{4-30}$$

As shown in Fig. 4-1, part of the source field is directed to RSOA, reflected, amplified and remodulated as the upstream signal. The power of the reflected field ε_r caused by the RSOA at the OLT is related to the source power P_s by:

$$P_r = \mathrm{Re}^{-2\alpha L} P_s, \tag{4-31}$$

where R describes the fraction of the power reflected and amplified by the RSOA. The total power before the receiver front end is:

$$\begin{aligned} P_t(t) &= [\varepsilon_r(t) + \varepsilon_b(t)] \cdot [\varepsilon_r(t) + \varepsilon_b(t)]^* \\ &= P_r(t) + P_b(t) + P_x(t) \end{aligned}, \tag{4-32}$$

where $P_r(t) = |\varepsilon_r(t)|^2$, $P_b(t) = |\varepsilon_b(t)|^2$, $P_x(t) = \varepsilon_r(t)\varepsilon_b^*(t) + \varepsilon_r^*(t)\varepsilon_b(t)$.

We next consider the case of transmitted bit '1' and bit '0' separately.

1) The Transmitted Signal is '1'

For the transmitted signal "1", the reflected power within the symbol interval is constant: $P_r = \text{Re}^{-2\alpha L} P_s$. The received optical field before the photo-detector is:

$$\varepsilon_t(t) = \varepsilon_r(t) + \varepsilon_b(t) = A_t(t)e^{j[\omega_0 t - \theta_t(t)]}, \tag{4-33}$$

where ε_r is the reflected signal field, ε_b is the RB field, $A_t(t)$ is the amplitude of the total received field, and $\theta_t(t)$ is the phase of the total received field. The Rayleigh backscattering noise power ψ_{RB-OOK} caused by OOK signal after the optical filter with transfer function $H(f)$ is

$$\Psi_{RB-OOK} = \int_{-\infty}^{\infty} |H(f)|^2 S_{\varepsilon_{b-OOK}}(f)df, \tag{4-34}$$

where $S_{\varepsilon_{b-OOK}}(f)$ is the Rayleigh backscattering field caused by OOK signal as given by Eqs. (4-28) and (4-29):

$$S_{\varepsilon_{b-OOK}}(f) = B \cdot S_\phi(f) \otimes \left\{ \frac{P_{av}d_{cy}}{2} \left(\frac{\sin(\pi f T_s d_{cy})}{\pi f T_s d_{cy}} \right)^2 \left[T_s + \sum_n \delta\left(f - \frac{n}{T_s} \right) \right] \right\} \tag{4-35}$$

As $\varepsilon_t(t)$ is a narrowband signal plus circular complex Gaussian (ccG) noise process, the p.d.f of its envelope is [26]:

$$p(A_t) = \frac{A_t}{\psi_{RB-OOK}} \exp\left[-\frac{\left(A_t^2 + A_r^2\right)}{2\psi_{RB-OOK}}\right] \cdot I_0\left(\frac{A_r A_t}{\psi_{RB-OOK}}\right), \qquad (4\text{-}36)$$

where A_r is the peak amplitude of the reflected signal ($A_r = \sqrt{P_r}$), and $I_0(\cdot)$ is the zero order modified Bessel function of the first kind. Assuming that the responsivity of the detector is unity, the total received current $i_1 = P_1 = |A_t|^2$, and the pdf of the received current is [26]:

$$p(i_1) = \frac{1}{2\psi_{RB-OOK}} \exp\left[-\frac{\left(i_1 + A_r^2\right)}{2\psi_{RB-OOK}}\right] \cdot I_0\left(\frac{A_r \sqrt{i_1}}{\psi_{RB-OOK}}\right) \qquad (4\text{-}37)$$

2) The Transmitted Signal is '0'

When the transmitted symbol is "0", the received signal is Rayleigh backscattering field alone. As the RB field is a ccG process, it can be written as the amplitude and the phase:

$$\varepsilon_b(t) = A_b(t)e^{j[\omega_0 t - \theta(t)]} \qquad (4\text{-}38)$$

where $A_b(t)$ and $\theta(t)$ are the envelope and phase of the Rayleigh backscattering field, respectively, and ω_0 is the central frequency of the system. As derived in [26], the p.d.f of the envelope of a normal process is a Rayleigh distribution:

$$p(A_b) = \frac{A_b \exp\left(-A_b^2 / 2\psi_{RB-OOK}\right)}{\psi_{RB-OOK}} \qquad 0 \le A_b \le \infty \qquad (4\text{-}39)$$

Since the detector current $i_0 = |\varepsilon_b(t)|^2 = A_b^2(t)$, the p.d.f of i_b is determined as a function of the pdf of $A_b(t)$ [42]:

$$p(i_0) = \frac{\exp(-i_0 / 2\psi_{RB-OOK})}{2\psi_{RB-OOK}} \qquad (4\text{-}40)$$

From Eq. (4-40), we see that the current caused by Rayleigh backscattering noise is a chi-square distribution with two degrees of freedom, which is consistent with the result in [50] when the polarization of the field is maintained.

3) Error Probability in OLT of the bidirectional System Using OOK/OOK Topology

Since the Rayleigh backscattering noise and the receiver noise induced by the detecting photodiode are independent, the error probability for bidirectional system using OOK/OOK topology can be written as [37]:

$$Pe = \frac{1}{4}\int_0^\infty Q\left(\frac{i-s}{\sigma_T}\right)p_{i_1}(i)di + \frac{1}{4}\int_0^\infty Q\left(\frac{s-i}{\sigma_T}\right)p_{i_0}(i)di, \qquad (4\text{-}41)$$

where $Q(z)$ is the complementary error function [42], s is the decision threshold which is chosen to be the average of the two received current $s = \left(\overline{I_r}/2 + \overline{I_b}\right)$, $p_{i_0}(i)$ and $p_{i_1}(i)$ are the probability density function of the received intensity for bit "0" and "1" respectively, and σ_T is the standard deviation of the receiver noise.

4.3.2 Error Probability for Bidirectional Systems Using DPSK/OOK

Topology

In the bidirectional optical system using DPSK/OOK topology, DPSK is used for downstream and OOK for upstream transmission. In the receiver at OLT, the square-law detection is used to detect the upstream OOK signal which is impaired by the Rayleigh backscattering field caused by the DPSK signal, while in the receiver at ONU, DPSK balanced receiver is used to detect the downstream DPSK signal which is impaired by the Rayleigh backscattering field caused by the upstream OOK signal. As the effects Rayleigh backscattering on the downstream DPSK signal is much smaller than that on the upstream OOK signal, here we consider the effects of Rayleigh backscattering on the error probability in OLT of DPSK/OOK topology only.

The power spectral density of the Rayleigh backscattering field caused by the downstream DPSK signal is

$$S_{\varepsilon_{s-DPSK}}(f) = P_{av}\left(\frac{2}{\pi} \cdot \frac{\Delta f}{\Delta f^2 + 4f^2}\right) \otimes d_{cy}T_s\left(\frac{\sin(\pi f T_s \cdot d_{cy})}{\pi f T_s \cdot d_{cy}}\right)^2, \qquad (4\text{-}42)$$

and the Rayleigh backscattering noise power is

$$\Psi_{RB-DPSK} = \int_{-BW}^{BW} S_{\varepsilon_{b-DPSK}}(f)df. \qquad (4\text{-}43)$$

In this case, the Rayleigh backscattering noise field interacts with the upstream

OOK signal and the expressions for the pdf of a mark and a space are similar to

that in Section 4.3.1. They are given by:

$$p(i_1) = \frac{1}{2\psi_{RB-DPSK}} \exp\left[-\frac{\left(i_1 + A_r^2\right)}{2\psi_{RB-DPSK}}\right] \cdot I_0\left(\frac{A_r\sqrt{i_1}}{\psi_{RB-DPSK}}\right), \tag{4-44}$$

$$p(i_0) = \frac{\exp\left(-i_0 / 2\psi_{RB-DPSK}\right)}{2\psi_{RB-DPSK}}, \tag{4-45}$$

The error probability can be calculated using Eq. (4-41) with the pdf of mark and

space given by Eqs. (4-44) and (4-45), respectively.

4.4   Simulation results

4.4.1   Results for Rayleigh Backscattering Caused by DPSK Signal

For standard single-mode fiber, we use the typical values for the Rayleigh

Backscattering coefficient $\alpha_s \cdot S$ to be -72dB around 1550 nm [49]. The total

length of the fiber is 20 km, the fraction of power reflected after amplification at

RSOA is $R = 0.1$, laser linewidth Δf = 50 MHz, bit rate B = 1 Gb/s. The optical

filter is an ideal bandpass filter matched with the signal spectrum with a full

bandwidth of $1.5/d_{cy}$ GHz. Fig. 4-3 shows the normalized power spectrum for

Rayleigh backscattering field with different duty cycle for systems based on

DPSK. From Fig.4-3, we see that the PSD of the Rayleigh backscattering field broadens as the duty cycle decreases.
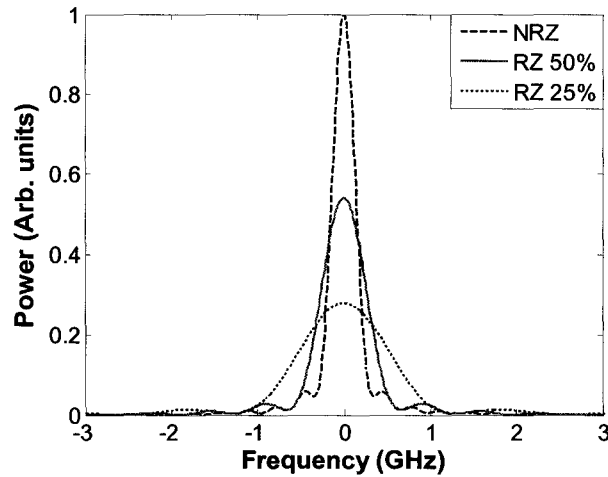
Fig. 4-3 PSD of Rayleigh backscattering field caused by DPSK signal. The peak value is normalized to be unit for NRZ-DPSK. Bit Rate = 1 Gb/s, Laser Linewidth =50 MHz.

4.4.2   Results for Rayleigh Backscattering Caused by OOK Signal

Fig. 4-4 shows the normalized spectra of the power of Rayleigh backscattering field caused by OOK signal. The system parameters are the same as in Section 4.4.1. We can see from Fig. 4-4 that, for the system based on OOK, as the duty cycle reduces, the main lobe of the PSD of the Rayleigh backscattering field reduces while the side lobes increase. In Fig. 4-5, the solid line and broken line show the pdf of the receiver power for NRZ-OOK and RZ-OOK with 50% duty cycle, respectively. Fig. 4-5a and 4-5b show the p.d.f of bit "1" and bit "0", respectively, for a system based on OOK obtained using Eqs. (4-37) and (4-40)

when the average transmitted power is -3 dBm. As can be seen, the p.d.f corresponding to bit "1" is much broader than that corresponding to bit "0", and as the duty cycle decreases, the p.d.f of the receiver power narrows while the peak increases.
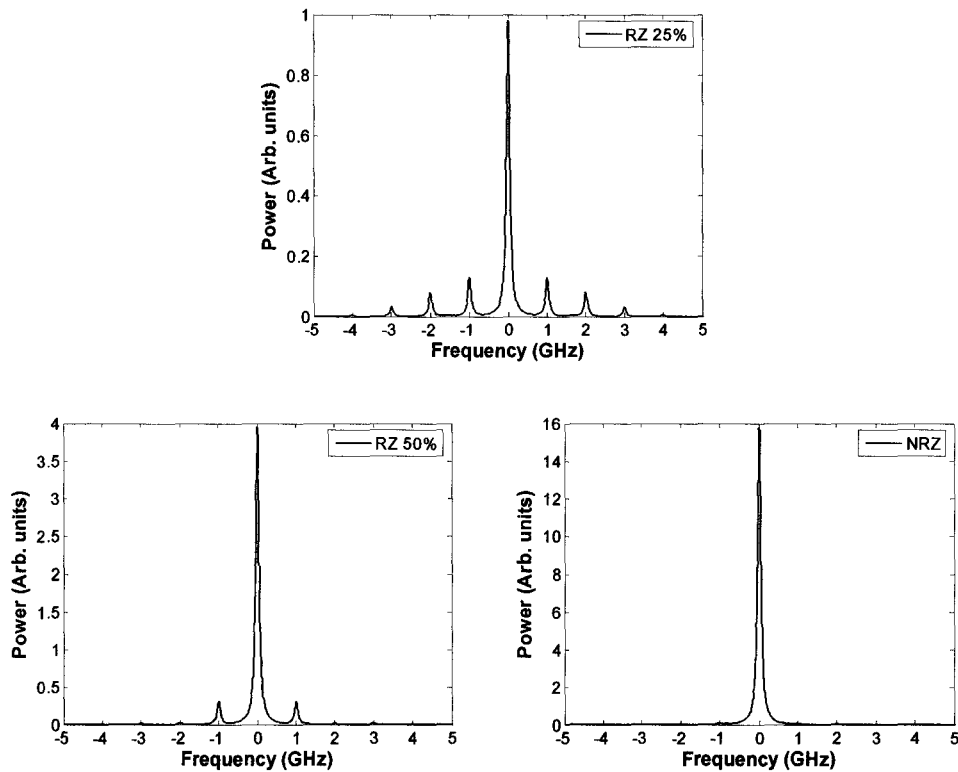
Fig. 4-4 Power Spectral Density of Rayleigh backscattering field caused by OOK signal. Bit Rate = 1 Gb/s, Laser Linewidth = 50 MHz, peak value of PSD is normalized to unity for RZ 25%.
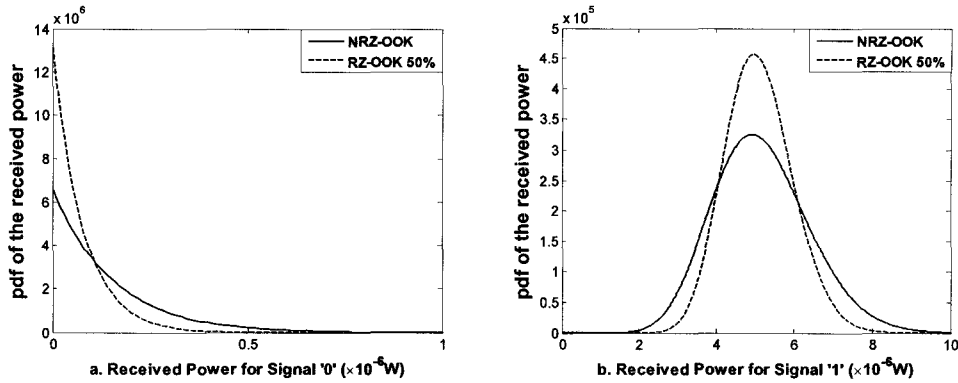
Fig. 4-5 Probability density function (pdf) of the received power for NRZ-OOK and RZ-OOK impaired by RB field. Fig. 4-5a shows the pdf of the received power when the transmitted data is zero, while Fig. 4-5b shows the pdf of the received power when the transmitted data is one. The average transmitted power is -3 dBm.

4.4.3 Error Probabilities for Bi-directional Systems Based on DPSK/OOK and OOK/OOK Topology

In this subsection, we calculate the error probability for bi-directional systems based on OOK/OOK as well as DPSK/OOK topology. Fig.4-6 shows the dependence of BER on the receiver power for systems using OOK/OOK topology and DPSK/OOK topology in OLT, respectively. The solid line shows the case NRZ-OOK/NRZ-OOK topology, the broken line with circle shows the case of NRZ-DPSK/NRZ-OOK topology. The standard deviation of the receiver noise is chosen to be $\sigma_T = 1.8 \times 10^{-6}$ A [52]. From Fig. 4-6, we see that, to reach the BER of 10^{-9}, the required receiver power for the bi-directional system using NRZ-DPSK/NRZ-OOK at OLT is around 9 dBm smaller than that required by the

system using NRZ-OOK/NRZ-OOK topology. In Fig. 4-7, we show the dependence of BER on the receiver power for RZ-OOK/RZ-OOK and RZ-DPSK/RZ-DPSK systems with duty cycle 50%. Comparing Fig. 4-7 with Fig. 4-6, we see that for both OOK/OOK and DPSK/OOK topology, the system performance is greatly enhanced by using RZ transmission.
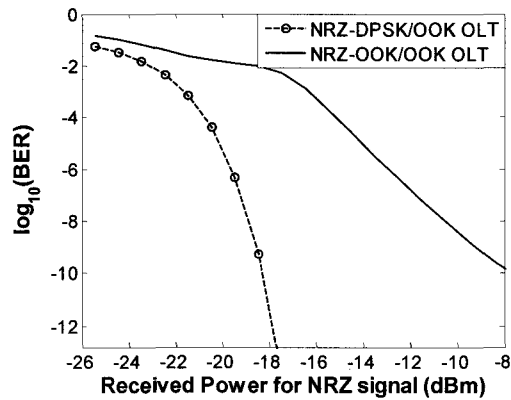
Fig. 4-6 Dependence of BER on the received power for bi-directional systems based on NRZ-OOK/NRZ-OOK Topology and NRZ-DPSK/NRZ-OOK Topology in OLT.
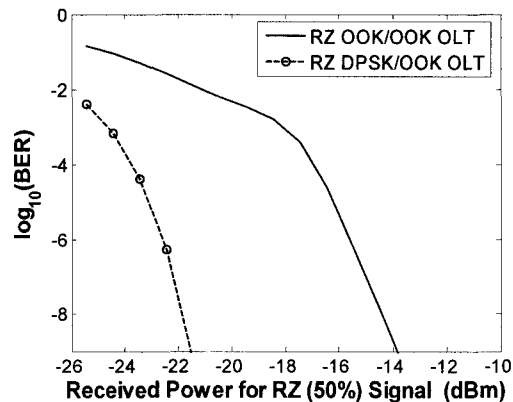
Fig. 4-7 Dependence of BER on the received power for bi-directional systems based on RZ-OOK/ OOK Topology and RZ-DPSK/ OOK Topology in OLT. The duty cycle is 50%.

4.5   Concluding Remarks

In summary, the network topology using DPSK for the downstream transmission and OOK for the upstream transmission in the FTTH PONs has been studied in this chapter. The statistical properties of Rayleigh backscattering field caused by DPSK signal and OOK signal has been studied, and error probabilities for bi-directional systems based on DPSK/OOK and OOK/OOK topology have been evaluated. Our results show that to reach the BER of 10^{-9}, the required receiver power for the bi-directional system using DPSK/OOK are 9 dBm smaller than that required by the system using OOK/OOK topology.

5

Two Dimensional Perturbation Theory for the Current Fluctuations Caused by Nonlinearity and Amplified Spontaneous Emission Noise in OOK Optical Transmission Systems

The introduction of erbium-doped fiber amplifiers (EDFAs) has realized the repeaterless optical transmission and no electronic regeneration takes place in the transmission line. The amplified spontaneous emission (ASE) noise of the in-line amplifiers can cause severe impairments for long-haul fiber optical communication systems. The interplay between the nonlinear Kerr effects and the ASE noise changes the statistical properties of the receiver noise, setting new limits for the maximum achievable error-free distance. For optical systems resorting to intensity-modulation/direct-detection (IM/DD) transmission schemes, it has been shown that

the interplay between fiber nonlinearity and ASE noise in the anomalous or zero group-velocity dispersion (GVD) enhances the noise spectrum through the modulation-instability process [13, 31]. While for the normally dispersive nonlinear fiber systems, only the in-quadrature noise power spectral density grows larger than the linear system, whereas the in-phase power spectrum is attenuated [15], and only the noise component that is in phase with the signal contributes to the overall signal variance.

In this chapter, we present a two dimensional perturbation method to calculate the variance of current fluctuations in a nonlinear dispersive fiber-optic system with inline amplifiers compensating the fiber loss. Our results show that for anomalously dispersive nonlinear systems, the current fluctuation is larger than that for a linear system with the same dispersion map, which is consistent with that in [31]; while for the normally dispersive nonlinear systems, the current fluctuation becomes smaller as compared with that of the linear system, consistent with Ref. [15]. The difference between our approach and that in Ref. [15] is that we study the impact of ASE noise and nonlinearity on a single pulse and on bit patterns used in practical systems, while in Ref. [15] the impact of ASE noise on a cw signal is studied. Our results show that the impact of the interplay between ASE noise and intra-channel cross-phase modulation (IXPM) on the noise current is much smaller than that between ASE noise and self-phase modulation (SPM) for which we have developed an analytical expression in this paper. In addition, the noise current in the dispersion managed systems has been studied, and our

results show that, for the dispersion managed system with an anomalously dispersive fiber as the first segment followed by a normally dispersive fiber, the current fluctuation caused by the interplay between ASE noise and fiber nonlinearity is smaller than that in a linear system, while the situation is opposite for a reverse dispersion managed system with a normal dispersive fiber as the first segment followed by an anomalously dispersive fiber. In addition, we have found that the current fluctuation caused by the interplay between ASE and IXPM is much smaller than that by the interplay between ASE and SPM.

In this chapter, Section 5.1 gives the detailed solution of the nonlinear Schrödinger equation for each term of the current noise using the two dimensional perturbation methods. In Section 5.2 we derived the closed-form analytical expression for the variance of the current fluctuations, and Section 5.3 gives the verification of the analytical results derived in Section 5.2 by the Monte-Carlo simulation of the nonlinear Schrödinger equation, and Section 5.4 summarizes our results.

5.1   Mathematical Analysis of Nonlinear Schrödinger Equation

The pulse propagation in optical fibers with periodic inline amplifiers is described by the lossless nonlinear Schrödinger equation (NLS):

$$j\frac{\partial u}{\partial z} - \frac{\beta_2(z)}{2}\frac{\partial^2 u}{\partial t^2} = -\gamma \exp(-w(z))|u|^2 u + j\lambda R(z,t), \qquad (5\text{-}1)$$

where u is the electric field envelop, $\beta_2(z)$ is the dispersion profile, $w(z) = \int_0^z \alpha(z)dz$, $\alpha(z)$ is the loss/gain profile, and $R(z,t)$ represents the ASE noise due to periodic amplification [5]:

$$R(z,t) = \sum_{n=1}^{N_a} \varepsilon(t)\delta(z - nL), \tag{5-2}$$

where N_a is the total number of inline amplifiers, and L is the amplifier spacing. The autocorrelation function of $\varepsilon(t)$ is

$$\left\langle \varepsilon(t) \cdot \varepsilon^*(t') \right\rangle = \delta(t'-t), \tag{5-3}$$

and the power spectral density of ASE noise is [52]

$$\lambda^2 = hf(G-1)n_{sp} \tag{5-4}$$

Let us consider a single pulse propagating down the fiber. The leading order solution to the nonlinear Schrödinger equation is [28]:

$$u_0 = \frac{\sqrt{P_0}T_0}{T_1}\exp\left(-\frac{t^2}{2T_1^2}\right), \tag{5-5}$$

where $T_1 = \sqrt{T_0^2 - js(z)}$, and $s(z) = \int_0^z \beta_2(s)ds$ \hfill (5-6)

To study the impact of the interplay between ASE noise and fiber nonlinear effects on the receiver current, we take λ and γ as small parameters, and expand the field in a series:

$$u = u_0 + \gamma u_\gamma + \lambda u_\lambda + \lambda\gamma u_{\lambda\gamma} + \cdots \tag{5-7}$$

where u_0 is the leading order solution when the nonlinearity is absent, $\gamma u_\gamma, \lambda u_\lambda$

and $\lambda \gamma u_{\lambda\gamma}$ represent the change in optical field due to fiber nonlinearity acting

alone, ASE noise acting alone, and the interplay between dispersion, nonlinearity

and ASE, respectively.

5.1.1   First-Order Solution when Nonlinearity and ASE Noise Acting Alone

The first-order corrections to the optical field due to nonlinearity has been studied

in [39] using a perturbation technique, and by considering the effects of only

SPM, the field can be expressed as

$$u_\gamma(z,t) = j\sqrt{P_0} \exp\left[-t^2 /\left(2T_0^2\right)\right]g(z,t) \qquad (5\text{-}8)$$

where

$$g(z,t) = \frac{T_0}{\sqrt{\pi}} \int_0^z \frac{\exp\left[-w(r) - \Delta(r)t^2\right]dr}{\sqrt{T_0^4 + 3s^2(r) + 2jT_0^2 s(r)}}, \qquad (5\text{-}9)$$

$$\Delta(r) = \frac{T_0^2 - js(r)}{T_0^2\left[T_0^2 + 3js(r)\right]}. \qquad (5\text{-}10)$$

To obtain the first order correction due to ASE noise acting alone, we

insert Eq.(5-7) into Eq.(5-1) and collecting all the terms that are proportional to λ

to obtain:

$$j\frac{\partial u_\lambda}{\partial z} - \frac{\beta_2(z)}{2}\frac{\partial^2 u_\lambda}{\partial t^2} = j\sum_{n=1}^{N_a} \varepsilon(t)\delta(z - nL). \qquad (5\text{-}11)$$

First, consider the effect of an amplifier located at $z = nL$. Taking the Fourier

transform of Eq.(5-11), we obtain

$$\tilde{u}_\lambda(\omega, L_{tot}) = \tilde{\varepsilon}(\omega) \cdot e^{jX\omega^2/2} \tag{5-12}$$

where $X = S(L_{tot}) - S(nL)$, $S(z) = \int_0^z \beta_2(z)dz$, and $\tilde{\varepsilon}(\omega)$ is the Fourier Transform of $\varepsilon(t)$.

An optical filter is used at the end of the transmission line with the transfer function:

$$H(\omega) = e^{-K\omega^2}, \tag{5-13}$$

where K is a constant related to the full bandwidth B_w as $K = 2\ln 2 / B_w^2$.

Multiplying the first-order noise field $\tilde{u}_\lambda(\omega, L_{tot})$ by $H(\omega)$ and taking the inverse Fourier transform, we obtain

$$u_\lambda(t, L_{tot}) = \frac{1}{2\sqrt{\pi Y}} \int_{-\infty}^{\infty} \varepsilon(t') \exp\left[-(t-t')^2/4Y\right]dt', \tag{5-14}$$

where $Y = K - jX/2$.

The auto-correlation function of the noise field can be obtained in the following method: Taking effect of the optical filter at the end of the transmission line, the expression for the noise field induced by the amplifier located at $z = nL$ is:

$$u_\lambda(t, z') = \begin{cases} \int_0^\infty \dfrac{\varepsilon(t')\exp\left[-(t-t')^2/4Y(z')\right]}{2\sqrt{\pi Y(z')}} dt', & for \quad z' > nL \\ 0, & elsewhere \end{cases} \tag{5-15}$$

where $Y(z') = K - \dfrac{j}{2}[s(z') - s(nL)]$.

Assuming the noise field is a stationary process, the autocorrelation function of the noise field is:

$$
\begin{aligned}
&\left\langle u_\lambda(0,z')u_\lambda^*(\tau,z'')\right\rangle \\
&= \int\limits_{-\infty}^{\infty}\int\limits_{-\infty}^{\infty}\left\langle \varepsilon(t')\varepsilon^*(t'')\right\rangle \frac{\exp\left[-t'^2/4Y(z')-(\tau-t'')^2/4Y^*(z'')\right]}{4\pi\sqrt{Y(z')Y^*(z'')}}dt'\,dt''
\end{aligned}
\tag{5-16}
$$

Let $Y_1 = Y(z')$ and $Y_2 = Y(z'')$, Eq. (5-16) is simplified to:

$$
\left\langle u_\lambda(0,z')u_\lambda^*(\tau,z'')\right\rangle = \frac{1}{4\pi\sqrt{Y_1 Y_2^*}}\int\limits_{-\infty}^{\infty}\exp\left[-\frac{t'^2}{4Y_1}-\frac{(\tau-t'')^2}{4Y_2^*}\right]dt'
\tag{5-17}
$$

Integrating Eq. (5-17), we obtain:

$$
\left\langle u_\lambda(0,z')u_\lambda^*(\tau,z'')\right\rangle = \frac{1}{2\sqrt{\pi(Y_1+Y_2^*)}}\exp\left[-\frac{\tau^2}{4(Y_1+Y_2^*)}\right],
\tag{5-18}
$$

where $Y_1 + Y_2^* = 2K + j\left[s(z'')-s(z')\right]/2$.

Let $K_c = K + j\left[s(z'')-s(z')\right]/4$, we have the autocorrelation function of the noise field

$$
\left\langle u_\lambda(t,z')\cdot u_\lambda^*(t+\tau,z'')\right\rangle = \begin{cases} \dfrac{\exp(-\tau^2/8K_c)}{2\sqrt{2\pi K_c}} & if \quad z'>nL,\quad z''>nL \\[2mm] 0 & otherwise \end{cases}
\tag{5-19}
$$

where $K_c = K + j\left[S(z')-S(z)\right]/4$.

Let $z'=z''=L_{tot}$, we have the autocorrelation function of the noise field at the end of the transmission line:

$$
\left\langle u_\lambda(t,L_{tot})\cdot u_\lambda^*(t+\tau,L_{tot})\right\rangle = \frac{\exp(-\tau^2/8K)}{2\sqrt{2\pi K}}
\tag{5-20}
$$

5.1.2   Second-Order Solution Due to Nonlinearity and ASE Noise Interplay

Substituting Eq. (5-7) into Eq. (5-1) and collecting all the terms that are proportional to $\lambda\gamma$, we obtain:

$$j\frac{\partial u_{\lambda\gamma}}{\partial z} - \frac{\beta_2(z)}{2}\frac{\partial^2 u_{\lambda\gamma}}{\partial t^2} = -\exp(-w(z))\cdot\left(2|u_0|^2 u_\lambda + u_0^2 u_\lambda^*\right) = F_1 + F_2, \quad (5\text{-}21)$$

where $F_1 = -2\exp[-w(z)]\cdot|u_0|^2 u_\lambda$, $F_2 = -\exp[-w(z)]\cdot u_0^2 u_\lambda^*$ (5-22)

For a linear Schrödinger equation with a source term F as given by

$$j\frac{\partial u}{\partial z} - \frac{\beta_2(z)}{2}\frac{\partial^2 u}{\partial t^2} = F(z,t) \quad (5\text{-}23)$$

Taking the Fourier transform on both sides of Eq. (5-23) and multiply each side by $e^{-jS(z)\omega^2/2}$, we have:

$$\frac{d}{dz}\left[j\widetilde{u}e^{-jS(z)\omega^2/2}\right] = \widetilde{F}(\omega,z)e^{-jS(z)\omega^2/2} \quad (5\text{-}24)$$

Take integration of Eq. (5-24), we have:

$$\widetilde{u}(\omega,z) = -j\int_0^z \widetilde{F}(\omega,z)\exp\left[j\left(S(z)-S(z')\right)\omega^2/2\right]dz' \quad (5\text{-}25)$$

Let $\beta(z,z') = s(z) - s(z')$, and take the reverse Fourier transform of Eq. (5-25), we have:

$$u(t,z) = -j\int_0^z F(t,z')\otimes h(t)dz', \quad (5\text{-}26)$$

where $\otimes$ denotes convolution, and

$$h(t) = F^{-1}\left(e^{j\beta\omega^2/2}\right) = \frac{1}{2\pi}\int_{-\infty}^{\infty} e^{j\beta\omega^2/2 + j\omega t} d\omega$$

$$= \sqrt{\frac{1}{2\pi(-j\beta)}} \exp\left(-\frac{jt^2}{2\beta}\right)$$

(5-27)

Insert Eq. (5-27) into (5-26), we have the solution for Eq. (5-23):

$$u(t,z) = -j\sqrt{\frac{1}{2\pi}}\int_0^z\int_{-\infty}^{\infty}\frac{F(z',t')}{\sqrt{-j\beta}}\exp\left(-\frac{j(t-t')^2}{2\beta}\right)dt'\,dz',$$

(5-28)

We assume that the decision is made at the central of bit slot, i.e., at $t = 0$.

Replacing $F(z,t)$ in Eq. (5-23) with F_1, the solution at $t = 0$ is given by:

$$u_{\lambda\gamma,1}(0,z) = A_0^{(1)}\int_0^z\int_{-\infty}^{\infty}A_1^{(1)}(z')e^{-B_1(z,z')\cdot t'^2}u_\lambda(t')dt'\,dz'$$

(5-29)

where

$$A_0^{(1)} = j\sqrt{\frac{1}{2\pi}}, \; A_1^{(1)} = \frac{2\exp[-w(z')]}{\sqrt{-j\beta}}\frac{P_0 T_0^2}{|T_1|^2}, \; B_1(z,z') = \frac{T_0^2}{|T_1|^2} + \frac{j}{2\beta}$$

(5-30)

Similarly, replacing $F(z,t)$ in Eq. (5-23) with F_2, we have the solution at $t = 0$:

$$u_{\lambda\gamma,2}(0,z) = A_0^{(2)}\int_0^z\int_{-\infty}^{\infty}A_1^{(2)}(z')e^{-B_2(z,z')\cdot t'^2}u_\lambda^*(t')dt'\,dz',$$

(5-31)

where

$$A_0^{(2)} = j\sqrt{\frac{1}{2\pi}}, \; A_1^{(2)} = \frac{\exp[-w(z')]}{\sqrt{-j\beta}}\frac{P_0 T_0^2}{T_1^2}, \; B_2(z,z') = \frac{1}{T_1^2} + \frac{j}{2\beta}$$

(5-32)

From Eqs.(5-29) and (5-31), we have the solution to the order of $\lambda\gamma$:

$$u_{\lambda\gamma}(t,z) = u_{\lambda\gamma,1}(t,z) + u_{\lambda\gamma,2}(t,z)$$

(5-33)

89

5.2   Variance of the current fluctuations

The electrical current generated by the photo-detector is related to the optical power by:

$$I = RP, \tag{5-34}$$

where R is the responsivity of the photo-detector, $P = |u|^2$ is the incident power on the photo-detector.

Eq.(5-7) can be written in the form:

$$u = u_d + \lambda u_\lambda + \lambda \gamma u_{\lambda \gamma}, \tag{5-35}$$

where $u_d = u_0 + \gamma u_\gamma$ represents the deterministic part of the field. Substituting Eq. (5-35) into Eq. (5-34), we obtain:

$$I = R|u_d|^2 + R\lambda \left(u_d u_\lambda^* + \gamma u_d u_{\lambda\gamma}^* + c.c \right) \\ + R\lambda^2 \left[|u_\lambda|^2 + \gamma^2 |u_{\lambda\gamma}|^2 + \gamma \left(u_\lambda u_{\lambda\gamma}^* + c.c \right) \right] \tag{5-36}$$

The first term in Eq. (5-36) represents the deterministic current, the second term (proportional to λ) represents the noise current due to signal-noise beating; and the last term (proportional to λ^2) represents the noise current due to noise-noise beating, which is usually quite small. Ignoring the last term, the variance of the noise current can be written as

$$\langle \delta I^2 \rangle = \langle I^2 \rangle - \langle I \rangle^2 = 2\lambda^2 R^2 |u_d|^2 \cdot \langle |u_\lambda|^2 \rangle$$

$$+ 2\lambda^2 \gamma R^2 \left[|u_d|^2 \langle u_\lambda^* \cdot u_{\lambda\gamma} \rangle + c.c \right] + 2\lambda^2 \gamma R^2 \left[u_d^{\,2} \langle u_\lambda^* \cdot u_{\lambda\gamma}^* \rangle + c.c \right]$$

$$+ 2\lambda^2 \gamma^2 R^2 |u_d|^2 \langle |u_{\lambda\gamma}|^2 \rangle + 2\lambda^2 \gamma^2 R^2 \left[u_d^{\,2} \langle u_{\lambda\gamma}^{*\,2} \rangle + c.c \right] \qquad (5\text{-}37)$$

$$= \sum_{i=1}^{5} \langle \delta I_i^2 \rangle,$$

where $\langle \delta I_i^2 \rangle$ represents the *ith* term on the right-hand side (RHS) of Eq. (5-37).

If the nonlinear effects are absent ($\gamma = 0$), from Eq.(5-37) we obtain

$$\langle \delta I^2 \rangle = 2\lambda^2 R^2 P_0 \langle |u_\lambda|^2 \rangle, \qquad (5\text{-}38)$$

where P_0 is the signal power. From Eq.(5-16), we have:

$$\langle |u_\lambda|^2 \rangle = \frac{1}{2\sqrt{2\pi K}} \qquad (5\text{-}39)$$

Combining Eqs.(5-39) and (5-38), we obtain:

$$\langle \delta I^2 \rangle = 2R^2 P_0 P_N, \qquad (5\text{-}40)$$

where P_N is the noise power given by:

$$P_N = \lambda^2 \int_{-\infty}^{\infty} |H(\omega)|^2 d\omega = \frac{\lambda^2}{2\sqrt{2\pi K}} \qquad (5\text{-}41)$$

Eq. (5-40) is the well-known result for the variance of signal-ASE beating [52], but here it is derived in a different way. $\langle \delta I_i^2 \rangle$ ($i = 2 \cdots 5$) represent the variance of the noise current due to signal-ASE-nonlinearity beating. To our knowledge, this was not studied before for the modulated signal, although modification of the

91

noise spectrum due to fiber nonlinearity for the cw signal has been studied before [15, 31]. From Eqs. (5-37) and (5-39), we have the expression for $\langle \delta I_1^2 \rangle$:

$$\left\langle \delta I_1^2 \right\rangle = \frac{R^2 \lambda^2 P_d}{\sqrt{2\pi K}}, \qquad (5\text{-}42)$$

where $P_d = |u_d|^2$. For $\langle \delta I_2^2 \rangle$, assuming the decision is done at $t = 0$, we obtain

$$\left\langle \delta I_2^2 \right\rangle = 2\lambda^2 \gamma R^2 P_d \left\langle u_\lambda^*(0, L_{tot}) u_{\lambda\gamma}(0, L_{tot}) \right\rangle + c.c$$

$$= 2\lambda^2 \gamma P_d A_0^{(1)} \int\limits_{nL}^{L_{tot}} \int\limits_{-\infty}^{\infty} A_1^{(1)}(z') e^{-B_1(L_{tot}, z')t'^2} \cdot \left\langle u_\lambda^*(0, L_{tot}) \cdot u_\lambda(t', z') \right\rangle dt' dz' + c.c$$

$$(5\text{-}43)$$

Inserting Eq. (5-15) into (5-43), we obtain:

$$\left\langle \delta I_2^2 \right\rangle = 2\lambda^2 \gamma R^2 P_d \int_{nL}^{L_{tot}} \frac{C_0(z') A_1^{(1)}(z') dz'}{\sqrt{B_1(L_{tot}, z') + 1/(8K_c)}} + c.c, \qquad (5\text{-}44)$$

where $C_0(z') = j/4\sqrt{\pi K_c}$, $\quad K_c = K + j[s(L_{tot}) - s(z')]/4$ $\qquad (5\text{-}45)$

Similarly we have the expression for $\langle \delta I_3^2 \rangle$:

$$\left\langle \delta I_3^2 \right\rangle = 2\lambda^2 \gamma R^2 \left[u_d^2 \left\langle u_\lambda^* \cdot u_{\lambda\gamma,2}^* \right\rangle + c.c \right]$$

$$= 2\lambda^2 \gamma R^2 \cdot u_d^2 \int_{nL}^{L_{tot}} \frac{C_1(z') A_1^{(2)*}(z') dz'}{\sqrt{B_2^*(L_{tot}, z') + 1/(8K_c)}} + c.c, \qquad (5\text{-}46)$$

where $C_1(z') = \dfrac{-j}{4\sqrt{\pi K_c}}$ $\qquad\qquad (5\text{-}47)$

The terms of $\langle \delta I_4^2 \rangle$ and $\langle \delta I_5^2 \rangle$ are proportional to $\lambda^2 \gamma^2$ and are given by Eqs. (5-48) and (5-49):

$$\left\langle \delta I_4^2 \right\rangle = 2\lambda^2 \gamma^2 R^2 P_d \left\langle \left| u_{\lambda\gamma} \right|^2 \right\rangle + c.c$$
$$= 2\lambda^2 \gamma^2 R^2 P_d \left(\left\langle \left| u_{\lambda\gamma,1} \right|^2 \right\rangle + \left\langle \left| u_{\lambda\gamma,2} \right|^2 \right\rangle \right) + c.c,$$

(5-48)

$$\left\langle \delta I_5^2 \right\rangle = 2\lambda^2 \gamma^2 R^2 u_d^{*2} \left\langle u_{\lambda\gamma}^2 \right\rangle + c.c$$
$$= \lambda^2 \gamma^2 R^2 u_d^{*2} \left[\left\langle u_{\lambda\gamma,1} u_{\lambda\gamma,2} \right\rangle + \left\langle u_{\lambda\gamma,2} u_{\lambda\gamma,1} \right\rangle \right] + c.c.$$

(5-49)

Close form expressions for $\left\langle \delta I_4^2 \right\rangle$ and $\left\langle \delta I_5^2 \right\rangle$ are obtained below:

For the term of $\left\langle \delta I_4^2 \right\rangle$, we have:

$$\left\langle \left| u_{\lambda\gamma,1} \right|^2 \right\rangle = \frac{1}{2\pi} \int_{nL}^{L_{tot}} \int_{nL}^{L_{tot}} \int_{-\infty}^{\infty} \int_{-\infty}^{\infty} A_1^{(1)}(z') A_1^{(1)*}(z'') e^{-B_1(z')t'^2 - B_1^*(z'')t''^2} \left\langle u_\lambda(t',z') u_\lambda^*(t'',z'') \right\rangle dt' dt'' dz' dz''$$
$$= \frac{1}{2\pi} \iiiint A_1^{(1)}(z') A_1^{(1)*}(z'') e^{-B_1(z')t'^2 - B_1^*(z'')t''^2} \frac{\exp\left(-(t'-t'')^2 / 8K_c \right)}{2\sqrt{2\pi K_c}} dt' dt'' dz' dz'',$$

(5-50)

where $K_c = K + j[S(z'') - S(z')]/4$.

Eliminating t' and t'' in Eq. (5-50) after the double integration, we have the expression for $\left\langle \left| u_{\lambda\gamma,1} \right|^2 \right\rangle$:

$$\left\langle \left| u_{\lambda\gamma,1} \right|^2 \right\rangle = -\frac{1}{2} \int_{nL}^{L_{tot}} \int_{nL}^{L_{tot}} \frac{A_1^{(1)}(z') A_1^{(1)*}(z'')}{2\sqrt{2\pi K_c} \sqrt{\alpha_1 \alpha_3}} dz' dz'',$$

(5-51)

where

$$\alpha_1 = B_1(L_{tot}, z') + \frac{1}{8\kappa_{c1}}, \alpha_3 = B_1^*(L_{tot}, z'') + \frac{1}{8\kappa_{c1}} - \frac{1}{64\kappa_{c1}^2 \cdot \alpha_1}.$$

(5-52)

In the same way, we have the expression for $\left\langle \left| u_{\lambda\gamma,2} \right|^2 \right\rangle$:

$$\left\langle \left| u_{\lambda\gamma,2} \right|^2 \right\rangle = -\frac{1}{2} \int_{nL}^{L_{tot}} \int_{nL}^{L_{tot}} \frac{A_1^{(2)}(z')A_1^{(2)*}(z'')}{2\sqrt{2\pi K_c^*}\sqrt{\alpha'_1 \alpha'_3}} dz' dz'', \qquad (5\text{-}53)$$

where

$$\alpha'_1 = B_2(L_{tot},z') + \frac{1}{8K_c^*}, \alpha'_3 = B_2^*(L_{tot},z'') + \frac{1}{8K_c^*} - \frac{1}{64K_c^{2*}\cdot\alpha'_1}. \qquad (5\text{-}54)$$

Using the same method as to derive $\left\langle \delta I_4^2 \right\rangle$, we can get the expression

for $\left\langle \delta I_5^2 \right\rangle$:

$$\left\langle \delta I_5^2 \right\rangle = \lambda^2 \gamma^2 u_d^{2*} \left\langle u_{\lambda\gamma}^2 \right\rangle + c.c = \lambda^2 \gamma^2 u_d^{2*} \left(M_1 + M_2\right) + c.c, \qquad (5\text{-}55)$$

where

$$M_1 = -\frac{1}{2} \int_{nL}^{L_{tot}} \int_{nL}^{L_{tot}} \frac{A_1^{(1)}(z')A_1^{(2)}(z'')}{2\sqrt{2\pi K_c}\sqrt{\chi_1 \chi_3}} dz' dz'', \qquad (5\text{-}56)$$

$$M_2 = -\frac{1}{2} \int_{nL}^{L_{tot}} \int_{nL}^{L_{tot}} \frac{A_1^{(2)}(z')A_1^{(1)}(z'')}{2\sqrt{2\pi K_c^*}\sqrt{\chi'_1 \chi'_3}} dz' dz'', \qquad (5\text{-}57)$$

$$\chi_1 = B_1(L_{tot},z') + \frac{1}{8K_c}, \chi_3 = B_1(L_{tot},z'') + \frac{1}{8K_c} - \frac{1}{64K_c^2 \cdot \chi_1}, \qquad (5\text{-}58)$$

$$\chi'_1 = B_2(L_{tot},z') + \frac{1}{8K_c^*}, \chi'_3 = B_2(L_{tot},z'') + \frac{1}{8K_c^*} - \frac{1}{64K_c^{*2}\cdot\chi'_1}. \qquad (5\text{-}59)$$

So far, we have considered the impact of a single amplifier located as

$z = nL$. The variance of current fluctuations due to all the amplifiers can be

obtained by adding the variance of each of the amplifier located at

$z = nL$, $n = 1, \cdots N_a$ since they are statistically independent.

5.3   Numerical verifications

To validate the analytical model as given in Eq.(5-37), we have carried out the numerical simulation of the nonlinear Schrödinger equation for a long-haul fiber-optic system with the following parameters: nonlinear coefficient = 2.43 $W^{-1}km^{-1}$, wavelength = 1.55 μm, fiber loss = 0.2 dB/km, pulse width (FWHM) = 50 ps, bit rate = 10 Gb/s, spacing between amplifiers = 80 km, n_{sp} =1, and computational bandwidth = 24 THz. An ideal optical filter with transfer function $H(\omega) = e^{-K\omega^2}$ ($K = 2.5 \times 10^{-23}$) is inserted at the end of the transmission line. A single Gaussian pulse is launched into the fiber with a peak power 3 mW. Monte-Carlo simulations of the nonlinear Schrödinger equation are carried out using the split-step Fourier method with 2000 realizations to compute the numerical variance of the peak power.

Firstly, we use a single fiber between two amplifiers. Fig. 5-1 shows the normalized standard deviation of the current fluctuation $\sigma = \sqrt{\langle \delta I^2 \rangle} \big/ \langle I \rangle$ as a function of the propagation distance when the fiber dispersion is anomalous. The solid line is obtained by numerical simulation from the nonlinear Schrödinger equation, the dashed line is obtained by our analytical results given by Eq.(5-37). Fig.5-2 shows the normalized standard deviation of the current fluctuation as a function of the propagation distance when the fiber dispersion is normal. From Fig. 5-1 and 5-2, we see that the variance of the current fluctuation is smaller than

that of a linear system when the dispersion is normal, while it is larger when the

dispersion is anomalous, consistent with Refs. [15] and [31].

Fig. 5-1.Normalized standard deviation of the current fluctuation for anomalously dispersive

fibers. The solid line and dashed line show the numerical simulation and analytical results,

respectively. The linear part considers only the ASE noise.
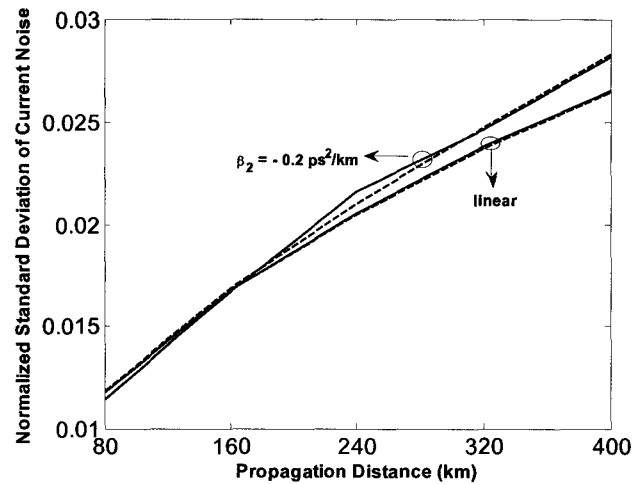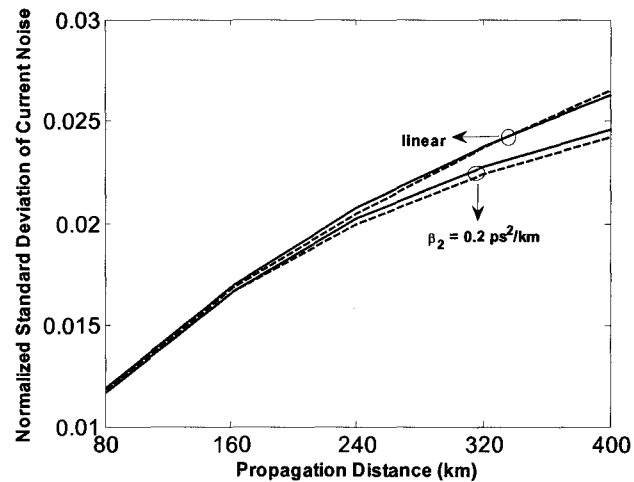

Fig.5-2. Normalized standard deviation of the current fluctuation for normally dispersive fibers.

The solid line and dashed line show the numerical simulation and analytical results, respectively.

The linear part considers only the ASE noise.

So far we have considered the impact of nonlinearity and ASE noise on a single pulse. In a typical IM/DD system, there is a nonlinear interaction due to IXPM between neighbouring pulses. To study the combined effect of IXPM and ASE noise, we have carried out the Monte-Carlo simulation of NLS equation with 17 bits with a bit period of 100ps. The central bit is fixed to be '1' and all the other bits are varied randomly in each realization. 2000 realizations are carried out in the Monte-Carlo simulation, and in each realization, the ASE noise seed and the bit pattern are random. We first perfom Monte-Carlo simulations by setting $n_{sp} = 1$ and calculated the normalized variance σ_{tot}^2. Next, we set $n_{sp} = 0$ and perform Monte-Carlo simulation to calculate the normalized variance σ_{NL}^2 due to IXPM and intra-channel four-wave mixing (IFWM) in the absence of ASE noise. The normalized standard deviation of current fluctuations due to the interplay between ASE, SPM &IXPM is given by $\sqrt{\sigma_{tot}^2 - \sigma_{NL}^2}$.

We consider the dispersion managed systems consisting of two sections of equal length between amplifiers. In Fig.5-3, the dispersion of the first section and that of the second section is equal in magnitude but opposite in sign, so that the accumulated dispersion between amplifiers is zero. We changed the dispersion coefficient of the first fiber segment from negative to positive and studied the dependence of the current fluctuation on the dispersion coefficient. The solid line shows the current fluctuations in the linear system, the dotted line shows the current fluctuation caused by SPM alone with single pulse launched into the

nonlinear system, and the dashed line shows the current fluctuation caused by

SPM and IXPM with 17 bits launched into the system. From Fig.5-3, we see that

for dispersion managed systems with anomalous dispersion fiber as the first

section, the variance of the current fluctuations is smaller than that of a linear

system if the first fiber segment has anomalous dispersion, while it is larger if the

first segment has normal dispersion. Again, the impact of ASE-IXPM interplay is

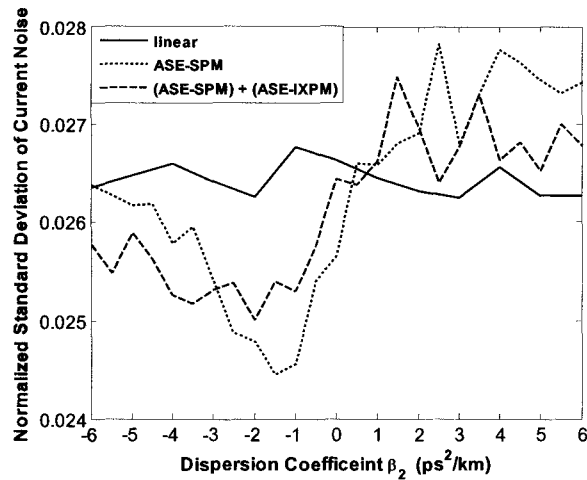quite smaller than that of the impact of ASE-SPM interplay.

Fig. 5-3 Numerical simulation of the nonlinear Schrödinger equation for dispersion-managed

systems. The dispersion coefficient of the first fiber section and the second fiber section are equal

in magnitude and opposite in sign. The x-axis is the dispersion coefficient of the first fiber section,

and the y-axis is the normalized standard deviation of the current fluctuation. Dotted line shows

the current fluctuation caused by the interplay between ASE and SPM alone with a single pulse.

Dashed line shows the current fluctuation caused by the interplay between ASE and SPM and

IXPM with 17 pulses. Solid line shows the current fluctuation in a linear system.

98

5.4   Concluding Remarks

In summary, the combined effects of fiber nonlinearity and amplifier spontaneous emission noise on the receiver current have been studied in a dispersive optical system. Closed-form analytical expressions have been derived for the variance of the current fluctuations, and are verified by the numerical simulation of the nonlinear Schrödinger equation. Our results show that for a fiber with normal dispersion, the variance of the current fluctuations is smaller than that in a linear system, while for a fiber with anomalous dispersion, it is larger than that in a linear system, which are consistent with the results in [31] and [15]. For a dispersion managed system where the first fiber segment has anomalous dispersion followed by a fiber segment having normal dispersion, the variance of the current fluctuation is smaller than that of a linear system, while the variance of the current fluctuation is larger than that of a linear system when the first fiber segment has normal dispersion and the second fiber segment has anomalous dispersion. Our results also show that the noise current caused by the interplay between ASE noise and IXPM is much smaller than that caused by the interplay between ASE noise and SPM.

6

Conclusions

In conclusion, for the long-haul fiber-optic communication systems, we have

derived an analytical expression for the variance of ASE induced nonlinear phase

noise including the effects of SPM and IXPM in dispersion-managed transmission

systems using DPSK modulation format, and validated this expression by numerical

simulation of the nonlinear Schrödinger equation. We have also developed the semi-

analytical expressions for the error probability for systems based on DPSK and

OOK. The optimum pre-compensation lengths for DPSK and OOK formats are

calculated and it is shown that optimizing the pre-compensation length for both

DPSK and OOK formats can both improve the performance. Under the optimized

conditions, the performance of DPSK and OOK formats in our system is studied

and compared for different launch powers. Our results show that to achieve the

given BER of 10^{-9}, the difference in SNR between systems based on DPSK and

OOK is around 3 dB when the launch power is small in agreement with the linear

theory. However, as the launch power increases, the SNR difference increases

implying that a system based on DPSK is more tolerant to nonlinear impairments than OOK. We have compared the performance of a system using resonant and non-resonant dispersion maps, and results show that the performance can be significantly improved for both formats if the non-resonant dispersion map is used.

The properties of Rayleigh Backscattering caused by DPSK signal and OOK signal have been studied for high-speed bidirectional FTTH passive optical networks. The analytical expressions for the error probabilities for bidirectional systems using OOK/OOK topology and DPSK/OOK topology have been evaluated, for the first time to our knowledge, including the effects of laser phase noise and the non-stationary modulation effects. Our results show that to reach the BER of 10^{-9}, the required receiver power for the bi-directional system using DPSK/OOK are much smaller than that required by the system using OOK/OOK topology.

The combined effects of fiber nonlinearity and amplifier spontaneous emission noise have been studied in a dispersive optical system. Closed-form analytical expressions have been derived for the variance of the current fluctuations, and are verified by the numerical simulation for various systems. Our results show that for a normally dispersive system, the current fluctuation is smaller than that in the linear system, and for an anomalously dispersive system, the power fluctuation is larger than that in the linear system.

Bibliography

[1] P. Mamyshev and N. Mamysheva, "Pulse-Overlapped Dispersion-managed Data Transmission and Intrachannel Four-wave Mixing," *Opt. Lett.*, vol.24, pp. 1454-1456, 1999.

[2] A. Gnauck and P. Winzer, "Optical Phase-Shift-Keyed Transmission," *J. of Lightwave Technol.*, vol. 23, pp.115-130, 2005.

[3] J. P. Gordon and L. F. Mollenauer, "Phase noise in photonic communications systems using linear amplifiers," *Opt. Lett.*, vol.15, pp. 1352-1353, 1990.

[4] A. G. Green, P. P. Mitra, and L. G. L. Wegener, "Effects of chromatic dispersion on nonlinear phase noise," *Opt. Lett.*, vol.28, pp.2455-2457, 2003.

[5] S. Kumar, "Impact of dispersion on nonlinear phase noise in optical transmission systems", *Opt. Lett.*, vol.30, pp.3278-3280, 2005.

[6] X.Wei and X.Liu, "Analysis of intrachannel four-wave mixing in differential phase-shift keying transmission with large dispersion," *Opt. Lett.*, vol. 28, pp.2300-2302, 2003.

[7] K. P. Ho, "Error probability of DPSK signals with intrachannel four-wave-mixing in highly dispersive transmission systems," *IEEE Photon. Tech. Lett.*, vol. 17, pp.789-791, 2005.

[8] P. J. Duthie, M. J. Wale, I. Bennion and J. Hankey, "Bidirectional Fiber-Optic Link Using Reflective Modulation," *Electron. Lett.*, Vol. 22, pp.517-518, 1986.

[9] J. Prat, C. Arellano, V. Polo, and C. Bock, "Optical Network Unit based on a bidirectional reflective semiconductor optical amplifier for fiber-to-the-home networks," *IEEEPhoton.Tech. Lett.*, vol. 17, pp.250-252, 2005.

[10] J. Prat, V. Polo, C. Bock, C. Arellano, and J. Vegas Olmos, "Full-duplex single fiber transmission using FSK downstream and IM remote upstream modulation for Fiber-to-the-home," *IEEE Photon.Tech. Lett.*, vol. 17, pp.702-704, 2005.

[11] R. Laming, M. Farries, L. Reekie, D. Payne, P. Scrivener, F. Fontana, and A. Righetti, "Efficient pump wavelengths of erbium-doped fiber amplifiers," *Electron. Lett.*, vol. 25, pp.12-14, 1989.

[12] D. Marcuse, "Noise Properties of four-wave mixing of signal and noise," *Electon. Lett.*, vol. 30, pp. 1175-1177, 1994.

[13] A. Mecozzi, "Long-distance transmission at zero dispersion: combined effect of the Kerr nonlinearity and the noise of the in-line amplifiers," *J. Opt. Soc. Am. B*, vol. 11, pp. 462-469, 1994.

[14] R. Hui, and M. O'Sullivan, "Noise squeezing due to Kerr effect nonlinearities in optical fibers with negative dispersion," *Electon. Lett.,* vol. 32, pp. 2001-2003, 1996.

[15] M. Midrio, "Statistical properties of noisy propagation in normally dispersive nonlinear fibers," *J. Opt. Soc. Am. B*, vol. 14, pp. 2910-2914, 1997.

[16] A. H. Gnauck, X. Liu, X. Wei, D. M. Gill, and E. C. Burrows, "Comparison of modulation formats for 42.7-Gb/s single-channel transmission through 1980 km of SSMF," *IEEE Photon. Technol. Lett.,* vol. 16, pp. 909-911, 2004.

[17] L. Moller, Y. Su, C. Xie, X. Liu, J. Leuthold, D. Gill and X. Wei, "Generation and detection of 80-Gbit/s return-to-zero differential phase-shift keying signals," *Opt. Lett.*, vol.28, pp.2461-2463, 2003.

[18] X. Wei, X. Liu, S. Simon and C. McKinstrie, "Intrachannel four-wave mixing in highly dispersed return-to-zero differential-phase-shift keyed transmission with a nonsymmetric dispersion map," *Opt. Lett.*, vol.31, pp.29-31, 2006.

[19] S. Detti, G. Marchis and E. Iannone, *Coherent Optical Communication Systems,* John Wiley & Sons, 1995, pp. 322-330.

[20] T. Chikama, S. Watanabe, T. Naito, H. Onaka, T. Kiyonaga, Y. Onoda, H. Miyata, M. Suyama, M. Seino, and H. Kuwahara, "Modulation and demodulation techniques in optical heterodyne PSK transmission systems," *J. of Lightwave Technol.,* vol. 8, pp.309-325, 1990.

[21] K. P. Ho, "Asymptotic probability density of nonlinear phase noise," *Opt. Lett.*, vol.28, pp.1350-1352, 2003.

[22] A. Mecozzi, "Probability density functions of the nonlinear phase noise," *Opt. Lett.*, vol.29, pp.673-675, 2004.

[23] R. H. Cameron and W. T. Martin, "Transformations of Wiener integrals under a general class of linear transformations," *Trans. Amer. Math. Soc.* **58**, 184 – 219, 1945

[24] J. G. Proakis, *Digital Communications*, 4th ed. McGraw-Hill, New York, 2000.

[25] P. C. Jain, "Error probabilities in binary angle modulation," *IEEE Trans. Inform. Theory,* vol.IT-20, pp.36-42, 1974.

[26] D. Middleton, *An Introduction to Statistical Communication Theory*. New York: McGraw-Hill, 1960, pp.417.

[27] K. P. Ho, "Impact of nonlinear phase noise to DPSK signals: a comparison of Different Models," *IEEE Photon.Tech. Lett.*, vol. 16, pp.1403-1405, 2004.

[28] G. P. Agrawal, *Nonlinear Fiber Optics*. Academic, 1995, pp. 67-68.

[29] A. Hasegawa and W. F. Brinkman, "Tunable coherent IR and FIR sources utilizing modulation instability," *IEEE J. Quantum Electron.* QE-16, 496-497, 1980.

[30] K. Tai, A. Hasegawa, and A. Tomita, "Observation of modulation instability in optical fibers," *Phys. Rev. Lett.* vol. 56, 135-138, 1986.

[31] M. Yu, G. P. Agrawal, and C. J. McKinstrie, "Pump-wave effects on the propagation of noisy signals in nonlinear dispersive media," *J. Opt. Soc. Am. B*, vol. 12, pp. 1126-1132, 1995

[32] R. Hui, and M. O'Sullivan, "Noise squeezing due to Kerr effect nonlinearities in optical fibers with negative dispersion," Electron. Lett. vol. 32, pp.2001-2003, 1996.

[33] G. Kramer, and G. Pesavento, "Ethernet passive optical networks (EPON): building a next-generation optical access network," *IEEE Commun. Magazine*, vol. 40, pp.66-73, 2002

[34] J. Prat. P. E. Balaguer, J. M. Gene, O, Diaz, and S. Figuerola, *Fiber-to-the-Home Technologies*. Norwell, MA: Kluwer.

[35] A. Hartog, and M. Gold, "On the theory of backscattering in single-mode optical fibers," *J. of Lightwave Technol.*, vol. LT-2, pp.76-82, 1984.

[36] P. Gysel and R. Staubli, "Statistical Properties of Rayleigh Backscattered in Single-Mode Fibers ," *J. Lightwave Technol.*, Vol. 8, pp.561-567, 1990.

[37] P. Gysel and R. Staubli, "Spectral Properties of Rayleigh Backscattered Light from Single-Mode Fibers Caused by a Modulated Probe Signal," *J. Lightwave Technol.*, Vol. 8, pp.1792-1798, 1990.

[38] A. Mecozzi, "Limits to long-haul coherent transmission set by the Kerr nonlinearity and noise of the in-line amplifiers," *J. of Lightwave Technol.*, vol. 12, pp.1993-2000, 1994.

[39] S. Kumar and D. Yang, "Second-order theory for self-phase modulation and cross-phase modulation in optical fibers," *J. of Lightwave Technol.*, vol. 23, pp. 2073-2080, 2005.

[40] P. Humblet and M. Arizoglu, "On the bit error rate of lightwave systems with optical amplifiers," *J. of Lightwave Technol.*, vol. 9, pp. 1576-1582, 1991.

[41] S. Kumar, J. C. Mauro, S. Raghavan and D. Q. Chowdhury, "Intrachannel nonlinear penalties in dispersion-managed transmission systems," *IEEE J. Sel. Topics Quantum Electron.*, vol.8, pp.626-631, 2002.

[42] J. G. Proakis, *Digital Communications*, New York: McGraw Hill, 4th ed., 2000, pp. 44.

[43] M. Manna and E. Golovchenko, "FWM resonances in dispersion slop-matched and nonzero-dispersion fiber maps," *IEEE Photon. Tech Lett.*, vol. 14, pp. 929-931, 2002.

[44] K. P. Ho and H.C. Wang, "Comparison of nonlinear phase noise and intrachannel four-wave mixing for RZ-DPSK signals in dispersive transmission systems," *IEEE Photon. Tech. Lett.*, vol. 17, pp.1426-1428, 2005.

[45] R. D. Hall, R. A. Betts and J. P. Moss, "Bidirectional Transmission over 11 km of Single-Mode Optical Fiber at 34 MBit/s Using 1.3 um LEDs And Bidirectional Couplers," *Electron. Lett.,* Vol.21, pp.628-629, 1985.

[46] I. Yamashita, "The latest FTTH technologies for full service access networks," IEEE Asia Pacific Conference on Circuits and Systems, pp. 263 – 268, 1996.

[47] M. D. Feuer, J. Wiesenfeld, J. Perino, C. Burrus, G. Raybon, S. Shunk, and N. Dutta, "Single_Port Laser-Amplifier Modulators for Local Access," IEEE *Photon. Technol. Lett.,*Vol. 8, pp.1175-1177, 1996.

[48] S. Haykin and B. Veen, *Signal and Systems.* Wiley & Sons, 1999.

[49] R. Staubli and P. Gysel, "Crosstalk Penalties Due to Coherent Rayleigh Noise in Bidirectional Optical Communication Systems," *J. Lightwave Technol.,* Vol. 9, pp.375-380, 1991.

[50] R. Staubli and P. Gysel, "Crosstalk Statistical Properties of Single-Mode Fiber Rayleigh Backscattered Intensity and Resulting Detector Current," *J. Lightwave Technol.,*Vol. 40, pp.1091-1097, 1992.

[51] R. W. Tkach and A. R. Chraplyvy, "Phase Noise and Linewidth in an InGaAsP DFB Laser," *J. Lightwave Technol.,* Vol. LT-4, pp.1711-1716, 1986.

[52] G. P. Agrawal, *Fiber-Optics Communication Systems.* Wiley & Sons, 1997, pp. 170-175.